THE ASTROPHYSICAL JOURNAL, 284:643–662, 1984 September 15

THE STRUCTURE AND DYNAMICS OF THE OPEN CLUSTER M11

ROBERT D. MATHIEU[1]
Astronomy Department, University of California, Berkeley
Received 1982 September 22; accepted 1983 January 4

ABSTRACT

A complete contamination-free sample of M11 cluster members has been obtained by combining proper-motion data of McNamara, Pratt, and Sanders with magnitude and color information obtained from deep KPNO 4 m plates. Difficulties in proper-motion membership techniques have been studied, with the conclusion that independent membership criteria are crucial for work in regions where the field dominates over the cluster (e.g., in the outer cluster) or where the proper-motion precision is poor (as is often the case at the faint limit of a proper-motion study). Completeness corrections for the proper-motion sample have also been made, and the data have been supplemented with deep star counts from the 4 m plates.

The luminosity functions in the inner and outer regions of M11 have marked differences due to mass segregation in the cluster. The luminosity function of all observed cluster members is in good agreement with the field initial luminosity function for stars with masses greater than 1.6 $M_\odot$ but is somewhat deficient in lower mass stars. Correcting for mass-segregation effects through dynamical models substantially decreases this deficiency.

The radial surface-density distribution is similar to that found for globular clusters. Mass segregation is evident in the progressively greater central concentration with higher mass. Multi-mass equipartition King models fit the radial surface-density profiles very well, with an anisotropy term being necessary if the model tidal radius is to agree with the theoretical tidal radius. Models with complete energy equipartition best fit the data; the data cannot, however, rule out with certainty the possibility that the lower mass stars have not yet come to complete equipartition.

The red giants of M11 have a smaller central concentration than the massive (turnoff) main-sequence stars. However, the statistical significance of the distinction is only at the 90% confidence level. Mass loss from the red giants with subsequent relaxation is considered as a possible explanation. Observations indicate that mass loss rates of such giants are not sufficiently rapid, but the present picture of mass loss from giants remains uncertain. It is also argued that explanations based on non-coevality of stellar formation seem implausible on the basis of the short cluster relaxation time scale.

Subject headings: clusters: open — luminosity function — stars: stellar dynamics

I. INTRODUCTION

From a dynamical point of view, open clusters represent an exciting and challenging field of study, both in observation and theory. On the observational side, the first challenge is to isolate the cluster members from the general field. As open clusters are located in the galactic disk, they are usually projected against rich stellar backgrounds. Consequently, the statistical methods which were so effective for globular clusters are often not sufficiently powerful, and new methods must be found by which cluster members can be isolated. The second observational challenge is to study the internal kinematics of open clusters. A simple virial analysis shows that the expected internal velocity dispersions of typical open clusters are on the order of 1 km s^{-1}. Thus, relevant kinematic information (e.g., global velocity dispersion, velocity dispersion as a function of stellar mass, and degree of anisotropy) is very difficult to obtain.

On the theoretical side, open clusters are dynamically active systems. Unlike globular clusters and galaxies, where the two-body relaxation times are very much longer than the crossing times and the systems can be considered to be in quasi-static equilibrium, the crossing and relaxation times of open clusters are more commensurate with each other. Thus the evolution of the cluster velocity distribution due to stellar encounters cannot be treated independently from the orbital mixing of the distribution. Analytically, this means the Liouville and collision terms must be solved simultaneously. The situation is made even more interesting by the fact that members of young open clusters cover a large mass range, so single-mass models such as have been used in most analyses of globular clusters are not appropriate. While the presence of different stellar masses complicates theoretical models, it also provides an empirical means to study two-body relaxation processes and time scales.

Finally, open clusters are subject to significant transient dynamical influences such as tidal perturbations of passing molecular clouds and mass loss by massive members, as well as the long-term effects of the galactic tidal field and the presence of binaries in the cluster. Thus, the dynamics of open clusters represents a theoretical problem which is different in essential nature as well as magnitude from that encountered in systems whose dynamics are thought to be well understood.

The goal of this paper is to present a data set which is sufficiently comprehensive, complete, and contamination-free to act as an observational base upon which theoretical analyses can begin. The choice of M11 (NGC 6705; $l^{II} = 27.^{\circ}3$, $b^{II} = -02.^{\circ}8$) as the representative open cluster was based both on consideration of optimal characteristics for analysis and on practical considerations of available data. M11 is an excellent

[1] Now at the Center for Astrophysics.

cluster for study because (1) it is young enough for its members to have a significant mass range, and (2) it is rich enough to allow statistically significant conclusions to be drawn. (Unfortunately, however, the richness of the cluster reduces its applicability to the study of systems with similar crossing and relaxation times.) Furthermore, McNamara, Pratt, and Sanders (1977) have completed an excellent proper-motion study which is sufficiently complete and comprehensive to permit a serious study of the cluster.

In this paper we develop in detail a procedure for producing a complete, contamination-free sample of the members of M11. We first use this sample to examine the cluster luminosity function. We then examine in detail the spatial structure of the cluster and begin an analysis of the cluster dynamics through application of the dynamical theory developed for large-N systems.

II. OBSERVATIONS

a) *Proper Motions*

The proper motions and membership probabilities used in this analysis are taken from McNamara, Pratt, and Sanders (1977). Using 15 independent plate pairs taken with the Yerkes 40 inch (1 m) refractor, they measure proper motions for 1890 stars in an area of ~ 0.25 deg^2 centered on the cluster. The faintest stars measured were $V = 16$ ($M_V = 3.5$), roughly 5 mag below the main-sequence turnoff at $V = 11$ ($M_V = -1.5$). McNamara *et al.* divide the data into three groups of varying measurement precision, based on the number of plate pairs used to determine a proper motion. The average proper-motion precisions for each group are: group 1 (1 plate pair), $\sigma = 0\farcs140$ per century; group 2 (2–7 plate pairs), $\sigma = 0.072$; group 3 (8–15 plate pairs), $\sigma = 0.039$. The number of plate pairs upon which a star can be measured is in turn dependent on the star's brightness, so measurement precision tends to decrease with fainter magnitude.

Membership probabilities were computed by McNamara *et al.* using the procedure described by Sanders (1971). This method consists essentially of fitting two bivariate frequency distributions to the proper-motion distribution: a normal elliptical distribution for the field and a normal circular distribution for the cluster. For any given proper motion, the membership probability is taken to be the ratio of the cluster distribution frequency to the sum of the cluster and field frequencies. The quality of the cluster/field separation is quite high for the high-precision data but decreases markedly for the low-precision stars.

b) *Photometry*

Solomon and McNamara (1980) photographically measured magnitudes and colors for 506 of the 811 stars found by McNamara *et al.* to have membership probabilities greater than 50%. Their selection criteria for the measured stars are not rigid. For example, only 50% of the stars fainter than $V = 14.0$ were photometered, the completeness becoming worse for fainter magnitudes. While many of the bright stars not measured are crowded by neighbors, most of the fainter stars have no obvious characteristics that would hinder photometry. Thus selection effects in the sample of photometered stars cannot easily be determined and compensated for.

Furthermore, the criterion of 50% membership probability is arbitrary, and, as shown below, not entirely satisfactory. For both of the above reasons, it was decided to complete the photometry for all stars with membership probability greater than 10% (approximately 500 additional stars). The 10% level was chosen because (1) the number of cluster members with membership probability less than 10% is very small, and (2) the total number of stars with membership probability less than 10% is large, roughly 700 stars.

Four direct photographs of M11, taken on 1980 October 9 with the 4 m Mayall telescope at Kitt Peak National Observatory,[2] were kindly provided by Drs. Spinrad and Stauffer. Two of the plates were a IIa-D + GG 495 combination yielding photographic V magnitudes. The remaining two were a IIa-O + GG385 combination, yielding photographic B magnitudes. All exposures were two minutes in 2″ seeing conditions. Limiting magnitudes were roughly $V = 20$ and $B = 21$.

The photometric procedure was straightforward. The unknowns were scanned in groups of 125 stars with the Berkeley PDS machine, using a 40×40 raster pattern of 20 μm (0″.37) pixels centered on each star. Ninety standards taken from Johnson, Sandage, and Wahlquist (1956) were also scanned before and after each set of unknowns. The stability of the PDS during the 90–120 minute scanning session (standard-unknown-standard) was easily checked by monitoring the sky level, and negligible drift was found.

As even the faintest of the unknowns are high signal-to-noise objects on these deep plates, and as the utmost precision is not needed for this analysis, a very simple photometry algorithm was sufficient. The center of the star image was determined simply by taking the maximum density pixel in the central region of the scan. The sum $\sum$ of the pixel densities in an 11×11 grid around that point was then taken as the photometric diagnostic. This grid size was found to be the largest which did not overly degrade the photometry of faint stars with sky noise.

Magnitude-density calibration for each scan of unknowns was achieved by fitting a cubic polynomial to a time-adjacent scan of standard stars. A typical calibration curve is shown in Figure 1. It is clear that this photometry scheme breaks down at the brightest levels because of saturation of the stellar image. The loss of accuracy at the bright end is rapid; we adopt $V = 12.0$ and $B = 13.0$ as bright limits for this photometry. For stars fainter than these limits, the scatter about the fitted curve is constant with magnitude. The single-measurement rms errors determined by comparison of measurements from two plates were $\sigma_V = 0.05$ and $\sigma_B = 0.06$; this is consistent with the scatter in the calibration curve. Combination of the two plates in each bandpass gives the final errors of $\sigma_V = 0.03$, $\sigma_B = 0.04$, and $\sigma(B-V) = 0.05$. The photometry for the newly observed stars is given in Table 1. A complete compilation of all spatial, kinematic, and photometric data for M11 is available from the author.

Photometry for stars with $V < 12$ was obtained when available from other work (e.g., Johnson, Sandage, and Wahlquist 1956; W. E. Harris, private communication). For the few remaining bright stars, approximate V magnitudes were obtained from McNamara *et al*; colors were not available for these stars. However, these stars all have very high accuracy proper motions, so color-magnitude information is not essential for membership determination. Also, where necessary in the analyses below, a visual inspection of the KPNO plates was

[2] Kitt Peak National Observatory is operated by the Association of Universities for Research in Astronomy, Inc., under contract with the National Science Foundation.

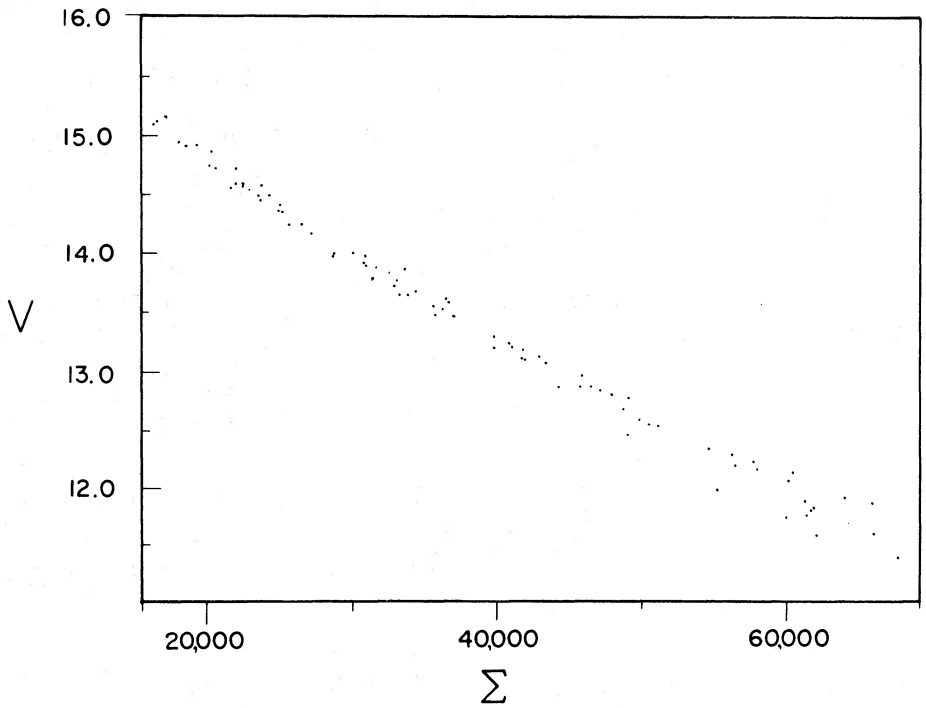

FIG. 1.—Calibration of photometric diagnostic $\sum$ (see text) vs. V; fainter than $V = 12.0, \sigma_V = 0.05$

sufficient to separate bright main-sequence stars and red giants. Finally, there were a few faint stars without photometry, because of crowding or other problems. Those with membership probability greater than 75% were included in the sample and given approximate V magnitudes from McNamara *et al.*; the remainder were excluded.

c) *Star Counts*

Because of the first-epoch plate magnitude limits, the proper-motion study could go only as faint as $V = 16$, roughly 1.4 $M_\odot$. For dynamical purposes, it is of interest to have information about the total mass and distribution of the lower mass stars. As the KPNO V plates reach roughly to $V = 20$, this information can be obtained by subtracting the proper-motion sample of cluster members from a total star count taken from one of these plates. The counting technique followed that of King *et al.* (1968). The count was done using a 3 cm (9.4) radius reseau divided into 36 octants and 30 annuli of 1 mm (18.″7) width. The counts per cell were never higher than 30 stars. Beyond 5′ from the cluster center the cluster counts were smaller than 2 standard deviations of the total count due to sampling error. Thus the star-count technique provides information only within a 5′ radius, to be compared with the 9.′6 radius of the proper-motion field. The limiting magnitude of the count was determined via photographic photometry of the faintest stars counted. This photometry was done using the University of California, Berkeley, photographic photometry package, described elsewhere (Mathieu and Spinrad 1981). The limiting magnitude of the count was found to be $V = 20$. (It should be noted that while the formal error in the photometry is very small, determinations of star-count limiting magnitudes are notorious for substantial systematic errors. The above estimate should only be trusted to ± 1 mag.)

These counts also provide an excellent means to search for any substantial absorption gradients across the cluster. The data were divided into quadrants and examined for radial asymmetries. No statistically significant variations were found. This is in agreement with an examination of the Palomar Sky Survey print of the region, which showed that, while M11 is surrounded by huge areas of extreme interstellar absorption, there are no obvious gradients across the cluster itself.

III. MEMBERSHIP DETERMINATION

a) *Technique*

Historically, proper-motion membership studies have been made with the intent of studying the color-magnitude characteristics of a given cluster. Clearly, in such work photometry could not be used as an independent membership criterion. However, for dynamical purposes it is the main body of stars that is of interest, while the rare anomalies are of no importance. As this body of stars has well-defined color-magnitude characteristics, i.e., the main sequence and giants, photometry represents an important additional tool for isolating cluster members where proper-motion techniques become weak (e.g., Upgren and Weis 1977; Upgren, Weis, and DeLuca 1979).

The use of proper motions to isolate cluster members has two inherent weaknesses. First, for mid-range membership-probability stars (30%–70%), the value of that probability is very sensitive to reduction techniques and measurement errors (McNamara and Schneeberger 1978). Second, stars exist in the field whose proper motions are more or less identical to those of the cluster members. Clearly, such stars cannot be identified as field members from proper motions alone. The degree of such field contamination depends on the precision of the proper motions, since the measurement dispersion defines the range of proper motions attributed to cluster members.

Thus a contamination-free cluster sample cannot be

TABLE 1

NEW PHOTOMETRY OF STARS IN M11 FIELD

Number[a]	V	$B-V$	Number	V	$B-V$	Number	V	$B-V$
6	13.44	0.48	297	15.79	1.54	534	13.92	1.67
11	15.47	1.52	298	15.52	0.82	537	13.07	0.56
29	14.87	2.20	300	15.25	2.20	548	15.39	1.04
34	13.98	1.72	301	15.17	1.88	551	15.92	1.30
36	15.31	0.89	303	14.54	1.79	554	15.47	0.72
45	13.64	1.45	304	15.75	1.71	563	16.23	1.69
52	15.21	2.22	308	14.50	1.02	564	15.68	2.07
56	15.61	1.69	312	15.21	2.16	572	14.98	0.59
64	15.45	0.84	316	15.25	2.10	576	14.39	2.05
65	14.47	1.66	317	15.38	1.59	578	14.99	1.63
70	14.82	1.44	327	15.14	0.83	580	14.97	2.01
78	15.49	1.68	330	15.33	0.78	584	14.96	1.51
86	14.79	2.20	331	14.79	0.60	585	14.52	2.12
94	14.72	1.81	335	14.59	0.52	595	15.08	1.05
96	15.17	1.75	338	14.70	1.68	600	15.87	1.83
97	15.55	0.96	345	14.62	2.03	602	15.48	0.72
98	14.55	1.63	346	15.27	0.70	604	15.20	0.69
99	15.48	1.78	347	15.04	0.64	606	14.97	2.03
106	15.63	1.38	350	15.24	1.11	610	15.14	1.81
110	15.50	1.11	351	15.87	0.85	614	15.42	0.73
118	15.71	0.94	353	15.59	1.12	618	14.95	0.63
123	15.93	1.01	357	15.19	0.86	620	15.04	1.87
130	14.86	2.14	361	13.38	0.46	622	14.52	0.60
133	14.71	1.31	366	15.17	0.70	623	14.48	1.63
144	13.79	1.39	367	15.61	0.95	627	15.51	1.02
147	15.46	1.10	370	15.09	0.68	629	14.57	0.47
164	14.51	0.49	371	15.15	2.13	636	15.54	0.72
168	15.45	0.85	374	15.34	1.90	641	14.46	0.91
174	15.11	1.62	378	15.36	1.03	652	14.18	0.48
186	15.39	0.64	380	15.02	2.20	656	15.12	1.80
191	15.29	1.98	382	15.56	1.52	657	15.28	0.77
192	15.46	1.63	388	15.32	1.70	661	13.98	0.57
193	15.78	0.88	393	15.02	1.86	670	15.19	0.69
194	14.73	2.20	394	14.71	0.94	678	13.82	0.91
195	15.14	1.58	400	15.85	0.80	679	15.61	1.02
196	14.68	1.66	403	15.91	1.47	684	14.55	0.54
200	14.28	0.50	415	14.56	0.51	687	15.22	1.14
202	15.21	0.75	417	15.84	1.98	695	14.91	0.61
205	15.37	1.64	422	15.26	1.00	701	15.84	1.06
211	14.17	0.89	423	14.96	0.65	707	15.37	0.80
213	14.94	0.58	429	14.60	2.00	709	14.56	0.54
214	14.77	0.53	432	15.19	0.61	711	14.48	0.67
222	15.16	1.01	433	15.13	0.86	712	15.55	0.76
223	16.05	1.16	435	15.89	1.04	716	12.92	0.41
224	15.01	0.77	439	15.16	0.61	718	13.19	0.44
229	15.20	1.68	440	15.48	1.77	721	15.03	0.83
230	15.90	0.56	442	15.46	0.73	726	15.61	1.68
231	14.65	0.53	444	15.51	1.06	728	14.97	0.83
238	15.05	0.68	447	14.94	2.40	729	15.58	1.29
240	15.61	1.37	450	15.01	0.62	733	15.34	1.66
241	15.00	1.54	456	15.21	0.67	740	13.50	0.51
244	15.83	0.82	459	15.29	1.77	741	14.71	0.51
249	14.98	0.56	465	14.87	1.84	742	15.18	0.69
251	15.08	0.67	466	14.89	2.03	743	14.63	2.07
254	15.20	2.20	471	15.06	0.57	746	15.01	0.61
261	14.97	1.40	479	15.00	0.70	747	13.51	0.41
263	15.35	0.76	480	14.87	1.69	749	15.32	0.65
264	15.65	1.47	482	16.11	1.00	755	14.89	0.63
269	14.93	2.08	483	15.51	0.76	758	15.22	0.92
272	15.76	1.60	484	14.70	0.57	760	13.80	0.54
273	15.66	1.26	492	15.00	0.63	761	13.84	0.44
274	14.52	2.20	493	14.90	0.98	762	15.21	0.76
275	14.69	0.93	496	14.89	2.03	766	13.48	0.41
276	15.01	1.74	500	15.56	0.79	769	15.36	1.82
278	14.52	1.20	502	15.18	0.94	772	13.88	0.53
279	15.68	0.80	504	15.65	0.77	774	13.00	0.34
282	15.35	0.71	518	13.77	0.42	776	13.05	0.35
283	14.75	1.94	525	15.72	0.89	784	14.90	0.72
287	15.23	1.60	526	14.24	1.25	785	15.44	0.75
292	15.68	1.61	531	15.25	0.00	788	13.16	0.46
293	15.18	1.58	533	13.39	1.53	789	13.17	0.48

TABLE 1—*Continued*

Number	V	$B-V$	Number	V	$B-V$	Number	V	$B-V$
796.....	16.09	1.08	1047.....	12.62	0.42	1277.....	13.75	0.48
797.....	14.34	2.24	1050.....	14.61	0.56	1278.....	13.84	0.46
798.....	15.45	0.72	1052.....	15.02	0.66	1280.....	15.39	0.55
802.....	15.12	0.64	1061.....	13.79	0.37	1288.....	15.10	0.63
806.....	15.06	0.68	1064.....	13.85	0.43	1291.....	14.57	0.61
814.....	14.88	0.88	1066.....	13.04	0.50	1293.....	15.24	0.92
820.....	14.46	0.44	1070.....	14.68	0.43	1300.....	15.83	0.89
829.....	15.30	0.97	1074.....	15.54	0.70	1302.....	14.24	0.68
834.....	15.37	0.74	1075.....	14.32	2.24	1308.....	14.89	0.59
835.....	14.67	1.54	1079.....	14.03	0.43	1317.....	14.44	0.53
838.....	13.54	0.37	1086.....	13.24	0.31	1320.....	15.04	0.47
839.....	15.35	0.71	1087.....	13.26	0.36	1322.....	14.03	1.36
840.....	12.14	0.29	1091.....	15.70	0.80	1324.....	14.71	0.68
845.....	14.99	0.65	1094.....	14.53	0.47	1326.....	14.53	0.39
846.....	15.25	0.69	1099.....	14.80	0.58	1333.....	12.59	0.39
848.....	13.61	0.43	1100.....	15.43	0.66	1335.....	15.16	0.63
853.....	15.58	0.77	1110.....	12.97	0.38	1337.....	15.19	0.67
856.....	13.42	0.31	1116.....	14.38	2.29	1342.....	15.41	0.78
857.....	14.55	2.28	1118.....	14.82	0.63	1346.....	15.03	0.75
858.....	15.19	0.66	1121.....	14.88	0.52	1347.....	14.58	0.52
859.....	15.30	1.60	1124.....	14.79	0.54	1351.....	14.23	0.56
875.....	14.92	0.73	1125.....	12.74	0.26	1352.....	13.90	0.47
876.....	15.08	0.60	1126.....	15.32	0.93	1355.....	14.15	0.46
880.....	15.48	0.98	1129.....	15.32	0.81	1357.....	14.08	0.58
883.....	15.22	0.59	1131.....	14.87	2.10	1363.....	14.07	0.48
901.....	13.89	0.44	1135.....	15.30	0.71	1371.....	15.24	0.92
902.....	14.13	0.47	1147.....	13.15	0.49	1372.....	14.07	0.43
903.....	13.46	0.40	1151.....	15.05	0.58	1375.....	15.46	0.80
904.....	15.55	0.97	1153.....	15.08	0.63	1376.....	14.25	1.85
909.....	15.18	0.66	1154.....	15.01	0.62	1379.....	15.37	0.69
915.....	13.43	0.31	1155.....	14.82	2.02	1384.....	15.22	1.51
918.....	13.37	0.49	1157.....	15.40	0.69	1389.....	13.49	0.50
923.....	14.28	0.30	1158.....	12.86	0.30	1390.....	14.77	0.98
927.....	13.04	0.39	1159.....	13.67	0.55	1402.....	14.90	0.50
929.....	15.72	1.16	1160.....	13.94	0.31	1409.....	15.52	0.74
932.....	14.17	0.44	1161.....	14.91	0.58	1414.....	13.85	0.41
937.....	15.31	0.67	1163.....	13.25	0.50	1416.....	15.41	0.88
940.....	15.39	0.67	1167.....	14.90	0.61	1422.....	14.51	1.79
943.....	14.25	0.60	1170.....	15.21	0.61	1426.....	13.13	0.37
944	15.56	0.74	1172.....	14.85	0.59	1428.....	14.44	0.43
945.....	15.01	0.73	1174.....	13.91	0.44	1441.....	14.99	0.86
946.....	13.81	0.71	1179.....	14.75	0.51	1444.....	14.95	0.69
947.....	15.11	0.52	1194.....	15.13	1.73	1445.....	15.18	0.93
953.....	12.89	0.35	1197.....	14.14	1.37	1450.....	15.43	0.72
955.....	15.52	2.31	1198.....	15.22	1.59	1451.....	15.49	1.05
956.....	14.57	0.62	1201.....	14.44	2.19	1464.....	14.24	0.63
957.....	14.83	0.53	1202.....	13.93	0.66	1467.....	14.77	0.53
961.....	15.22	0.74	1205.....	13.11	0.40	1473.....	13.40	2.45
964.....	14.32	0.40	1208.....	13.88	0.55	1476.....	15.30	0.77
969.....	14.32	0.40	1209.....	14.56	0.51	1477.....	15.13	2.03
972.....	15.22	0.67	1215.....	15.27	0.69	1479.....	15.22	1.50
975.....	15.21	0.75	1218.....	13.48	0.35	1481.....	13.81	0.47
976.....	15.28	0.69	1219.....	12.52	0.48	1482.....	15.54	1.07
980.....	15.53	0.81	1222.....	13.88	0.31	1485.....	14.60	1.54
984.....	14.21	0.47	1224.....	14.80	0.50	1486.....	15.12	0.67
986.....	13.73	0.55	1227.....	13.77	0.47	1490.....	12.88	0.27
1010.....	15.33	0.68	1229.....	15.19	0.60	1492.....	14.21	0.46
1018.....	15.31	0.75	1230.....	15.25	0.82	1494.....	14.30	0.52
1019.....	14.13	0.49	1231.....	14.18	0.43	1499.....	14.74	0.55
1020.....	13.19	0.41	1236	13.98	0.44	1500.....	14.57	0.55
1021.....	12.34	0.57	1238.....	15.04	0.69	1501.....	14.35	0.53
1023.....	14.64	0.71	1243.....	13.38	0.40	1502.....	15.30	0.70
1025.....	14.27	0.45	1245.....	13.00	0.44	1504.....	14.90	1.57
1028.....	14.94	2.09	1251.....	15.54	0.70	1505.....	12.60	0.45
1031.....	13.36	0.43	1254.....	15.39	0.94	1507.....	13.29	0.35
1033.....	13.53	0.47	1255.....	14.74	0.52	1508.....	15.25	0.86
1036.....	16.05	1.60	1262.....	15.52	0.67	1509.....	15.61	0.79
1038.....	15.33	1.77	1267.....	13.91	0.54	1511.....	15.22	0.61
1039.....	14.15	2.24	1268.....	13.55	0.73	1514.....	14.74	2.30
1042.....	15.25	0.64	1269.....	14.99	0.61	1517.....	15.53	0.89
1043.....	14.90	1.53	1272.....	12.82	0.37	1525.....	15.43	0.69
1045.....	14.85	0.67	1276.....	14.31	0.52	1531.....	14.31	0.48

TABLE 1—*Continued*

Number	V	$B-V$	Number	V	$B-V$	Number	V	$B-V$
1536.....	14.95	1.89	1705.....	15.27	1.06	1889.....	15.15	0.67
1539.....	14.80	0.55	1706.....	14.99	0.63	1891.....	14.86	0.48
1540.....	14.86	0.53	1712.....	16.28	1.39	1894.....	15.12	1.10
1543.....	14.95	0.71	1713.....	15.57	1.70	1897.....	14.73	1.88
1544.....	13.20	0.49	1718.....	14.93	0.77	1907.....	15.28	1.07
1545.....	15.23	0.89	1723.....	15.07	1.41	1908.....	14.46	1.76
1552.....	14.79	0.56	1735.....	14.50	0.70	1917.....	15.72	0.70
1553.....	15.45	1.06	1737.....	15.23	1.14	1923.....	14.43	2.29
1560.....	15.46	1.68	1738.....	14.91	0.66	1924.....	14.48	2.20
1561.....	14.87	1.54	1742.....	13.71	0.45	1928.....	14.51	2.13
1570.....	14.28	0.87	1746.....	15.09	0.63	1935.....	15.19	1.00
1571.....	14.77	1.74	1750.....	14.00	0.48	1943.....	15.19	1.73
1574.....	15.39	1.62	1752.....	15.31	1.46	1948.....	15.93	1.79
1575.....	15.32	0.69	1758.....	15.12	0.82	1949.....	14.83	1.69
1580.....	14.50	0.77	1762.....	14.98	1.67	1957.....	15.39	1.02
1590.....	14.86	0.87	1763.....	15.21	1.15	1963.....	12.98	1.56
1593.....	15.14	1.72	1767.....	14.78	0.95	1967.....	15.21	1.96
1596.....	15.26	0.54	1771.....	13.90	0.57	1970.....	14.87	2.24
1603.....	14.86	0.89	1776.....	14.80	0.56	1976.....	15.78	1.90
1611.....	14.12	0.44	1778.....	15.54	0.88	1979.....	14.72	0.78
1612.....	15.43	0.68	1779.....	15.09	1.79	1980.....	15.46	1.11
1613.....	14.87	0.59	1781.....	14.55	0.47	1981.....	15.53	1.03
1616.....	15.19	0.64	1783.....	14.97	0.72	1986.....	15.30	0.58
1618.....	15.65	0.73	1790.....	15.32	0.81	1991.....	14.84	2.30
1629.....	15.09	1.55	1792.....	15.42	1.10	1992.....	13.89	1.81
1632.....	15.02	2.24	1796.....	14.62	1.57	1994.....	13.57	1.58
1634.....	14.38	1.75	1808.....	14.61	0.77	1996.....	14.29	0.43
1639.....	14.06	1.57	1809.....	14.37	1.15	2006.....	15.12	1.85
1642.....	13.46	0.34	1811.....	14.64	0.74	2007.....	15.08	0.73
1644.....	14.95	0.58	1820.....	13.50	1.37	2008.....	14.96	1.86
1652.....	14.15	0.47	1821.....	13.40	0.41	2013.....	15.43	1.87
1659.....	14.37	0.45	1823.....	15.54	1.72	2017.....	15.48	0.73
1660.....	15.73	0.97	1830.....	14.62	0.68	2023.....	15.47	0.86
1663.....	15.27	2.00	1834.....	14.68	2.11	2027.....	15.52	2.10
1666.....	15.01	0.99	1836.....	15.32	0.95	2028.....	13.26	0.83
1668.....	14.93	0.98	1838.....	14.56	0.64	2031.....	14.97	1.32
1671.....	15.43	1.34	1839.....	15.41	1.01	2033.....	15.16	1.73
1672.....	14.07	0.43	1842.....	15.34	0.97	2036.....	13.96	1.30
1674.....	15.68	0.79	1843.....	15.63	1.82	2039.....	14.41	2.39
1680.....	15.47	0.67	1849.....	15.31	0.63	2040.....	12.95	0.28
1682.....	15.28	2.03	1853.....	15.41	0.79	2041.....	15.36	1.00
1683.....	14.36	2.02	1854.....	15.39	1.75	2043.....	15.30	1.67
1684.....	14.45	1.51	1860.....	15.42	0.74	2046.....	15.01	1.83
1687.....	14.47	1.43	1862.....	14.89	0.48	2058.....	13.20	0.56
1698.....	15.08	0.67	1872.....	15.00	1.78	2060.....	14.26	2.41
1701.....	15.92	0.94	1878.....	14.67	2.40			

[a] Reference number of McNamara, Pratt, and Sanders 1977.

obtained via proper-motion selection alone, particularly for faint stars where measurement precision is often low. Color-magnitude information represents an independent criterion for membership. The color-magnitude diagram of all stars with proper-motion membership probabilities greater than 10% is given in Figure 2. There are three clear groupings: the main sequence, the giants, and a large dispersed group of faint red stars. This last group comprises the stars to be edited from the sample of cluster members.

The principle on which the photometric determination of nonmembers is based is straightforward: all stars not falling on the main sequence or among the giants are classified as nonmembers. In practice, there are two complications. The first is the presence of binaries in the cluster, which tend to fall somewhat above the main sequence in a color-magnitude diagram. Being cluster members, they should not be edited from the sample. The second complication lies in the definition of the main sequence itself. Since proper-motion accuracies are often poorer for fainter stars, the quality of membership separation is correspondingly reduced. The result is that for fainter stars, the color-magnitude diagram becomes cluttered with nonmembers, and the main sequence can become poorly defined. This is evident in Figure 2.

The operational definition of the main sequence used in this paper is shown by the solid lines in Figure 2. For stars brighter than $V = 14$, the main sequence is well defined. For stars fainter than $V = 14$, the definition of the main sequence was determined by looking only at the central 2′ of the cluster. The small area reduces the field contamination significantly, while the high cluster density in the central regions provides a sufficient number of cluster members to define the main sequence. The width of the adopted main sequence is sufficiently liberal that few member binaries should be excluded.

As a check on this definition of the main sequence for $V > 14$, a thin strip to the red side of the main sequence was isolated for study. (This region is defined by the dashed line in Fig. 2.) The cluster was divided radially into three regions with outer radii of 2′, 6′, and 10′. The surface densities for each

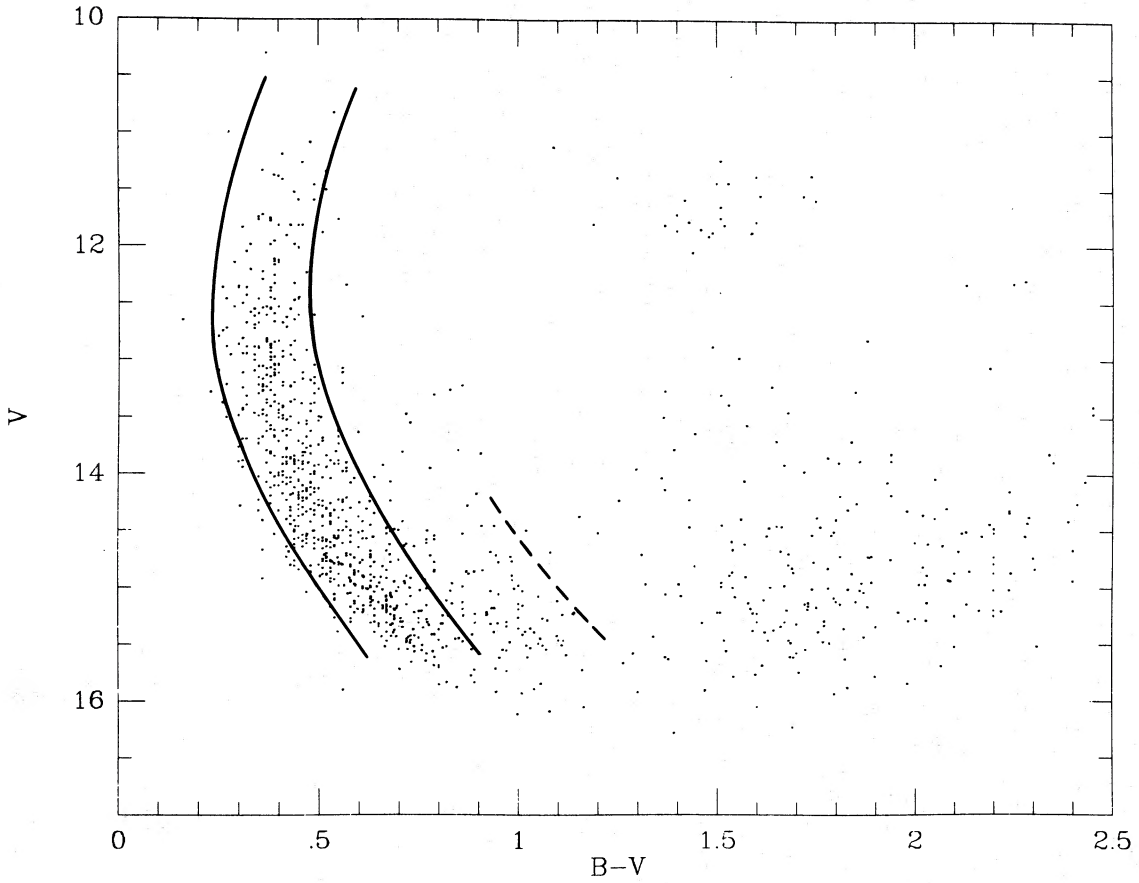

FIG. 2.—Apparent color-magnitude diagram of M11 for stars with proper-motion membership probabilities greater than 10%. Solid lines define adopted main sequence. For explanation of dashed line, see text.

spatial region of stars falling in the color-magnitude strip were 0.41 ± 0.29, 0.42 ± 0.12, and 0.41 ± 0.10, in units of arcmin^{-2}. It is evident that the distribution of these stars is uniform, implying that they are in fact members of the field.

b) Analysis

The essential question is, given proper-motion and color-magnitude data, how does one define the sample of cluster members? Traditionally, all stars above a given proper-motion membership lower limit have been identified as members. The values chosen for this lower limit range from 50% to 70% (e.g., McNamara and Sanders 1977; Chiu and van Altena 1981). Many cluster members have lower membership probabilities, however. A color-magnitude diagram of the M11 stars with membership probability between 10% and 50% shows a well-defined main sequence admidst the scatter of the field stars. Thus the trade-off in the choice of membership-probability cutoff is between purity and completeness of the cluster sample. For luminosity functions and density profiles, however, neither can be acceptably compromised. A high membership-probability cutoff unacceptably reduces the number of stars for study, particularly in the outer regions and for faint stars with lower precision proper motions, while a lower cutoff results in contamination, with unpredictable effects on the sample of "cluster" stars.

The addition of color-magnitude editing of field stars significantly reduces the problem, as one can be very liberal in the choice of cutoff—assuring high completeness—and then remove the contaminating field stars. In this study, a 10% membership-probability cutoff was selected (thus initially removing from consideration 40% of all stars with measured proper motions). This sample was then edited using the color-magnitude data. The difference in the resulting cluster-member sample from that obtained by simply choosing a 50% lower limit is significant. Considering first only the group 1 (low-precision proper motion) stars within a 10′ radius, there are 172 stars with membership probability greater than 50%, 81 of which are actually members as determined from their color-magnitude data. There are in addition 57 cluster members with membership probabilities between 10% and 50%. Thus simply choosing all stars with membership probability above 50% of the cluster sample would result in a 25% error in the determined number of members. That the error is only this large is largely fortuitous in that the field contamination of the group with membership probability above 50% is similar to the number of cluster members with membership probability below 50%. In fact, the sample with membership probability above 50% is half comprised of field stars. Thus any analysis of such data without color-magnitude editing would be misleading.

A similar analysis for stars in group 2 finds that 315 of the 383 stars above 50% membership probability are cluster members. Thirty-six additional members were found with membership probabilities between 10% and 50%. Thus, using a simple 50% cutoff results in a 9% overestimate of the cluster membership. Note that the error is a function of proper-motion precision and consequently stellar luminosity (see Table 2). Thus the use of variable-precision proper-motion

TABLE 2

PERCENT FIELD CONTAMINATION OF PROPER-MOTION CLUSTER SAMPLE VERSUS RADIUS AND MAGNITUDE

	Radius (pc)				
V	2	4	6	8	10
11–12.....	0	0	0	0	0
12–13.....	5	5	5	25	14
13–14.....	5	5	17	33	31
14–15.....	8	14	19	35	73
15–16.....	7	42	61	76	68

data and a single membership-probability lower limit as the membership criterion can lead to *differential* errors in luminosity functions, color-magnitude diagrams, etc.

The primary concern for dynamical work is the degree of field contamination as a function of radius. Table 2 gives the percentage of field contamination as a function of radius for the sample of stars with membership probability greater than 50%. The error in the number of members in the outer-regions determined from the proper-motion analysis alone can be higher than a factor 2. More to the point, the contamination is strongly dependent on radius, so again differential errors are introduced into the radial surface-density profiles.

Thus, unless the proper-motion data are of uniformly high quality, the importance of using photometry as an independent membership criterion cannot be overstated. If the quality of some fraction of the proper-motion data is low, the suggested procedure is to exclude the certain nonmembers (e.g., stars with membership probability below 10%) and from the remaining sample select members on the basis of color-magnitude information.

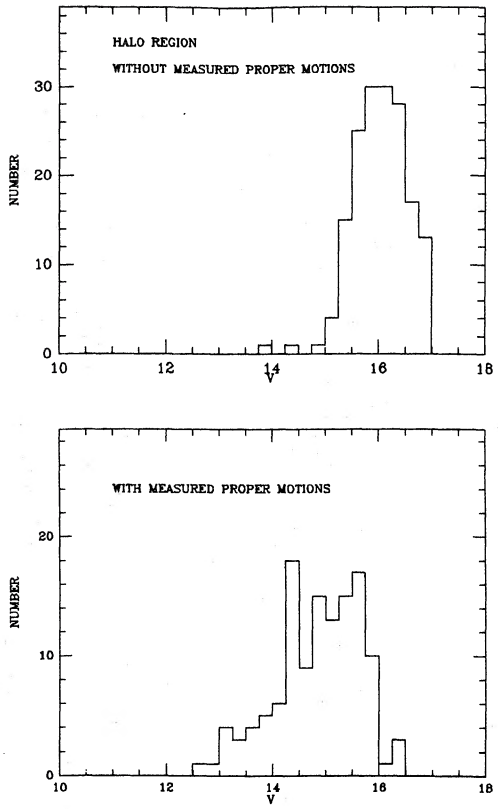

FIG. 3.—Histogram of magnitudes for stars ($V < 17$) in a selected region outside the cluster core, differentiating between stars with and without measured proper motions.

IV. COMPLETENESS

Incompleteness in the sample may exist for two reasons: plate-limit effects and crowding in the central regions. To estimate the former, a 50 arcmin^2 region north of the cluster core was examined on a KPNO V plate, which goes roughly 4 mag deeper than the $V = 16$ completeness limit claimed by McNamara *et al.* All stars in the region brighter than $V = 17$ (an approximate limit, as selection was based on visual inspection of the plate) were photometered. In Figure 3 histograms are given of the number distributions with magnitude of stars with and without measured proper motions. Clearly, the 100% completeness level is only $V = 15.0$, while for $V = 15.0$–15.5 the sample is 60% complete. Below $V = 15.5$, the sample is essentially too incomplete to be useful. In the luminosity-function analysis below, the faintest bin ($V = 15.0$–15.5) has included a completeness correction factor of 1.6.

In the core of the cluster (roughly within a radius of 2′), the situation is more complicated because of crowding. Crowding leads to (1) proper motions not being measured for some stars and (2) poor precision for crowded stars that are measured. The extent of the first effect can be estimated as in the outer region. Because of the superior quality of the KPNO V plate, it was taken to be uncrowded, i.e., no obscuration of one star by another. (The KPNO plates in fact come close to satisfying the approximate criterion of King *et al.* 1968, who find that crowding effects set in when about 1/50 of the plate area is covered by stellar images. Nonetheless, certainly some stars are in fact obscured.) As above, the number distributions with magnitude of stars in the central region with and without measured proper motions are given in Figure 4. Unlike the situation in the outer-region, some inner-region stars of all magnitudes have been missed in the proper-motion study, presumably because of crowding. The data in Figure 4 allow determination of the factor $F(V)$ necessary to correct the sample for stars missed as a result of crowding. The values of $F(V)$ applied to data inside 2′ are: $V < 12$, 1.22; $V = 12$–13, 1.20; $V = 13$–14, 1.28; $V = 14$–15, 1.37.

That crowding also affects proper-motion measurement precision can be seen by an examination of the radial surface-density distribution of field stars. In Figure 5 are given the radial surface-density distributions of stars with membership probability less than 10%, divided into four luminosity groups. (The photometry is taken from McNamara *et al.*; faint stars for which McNamara *et al.* have no magnitudes are included in the faintest group.) All groups show a marked increase in surface density in the cluster core. The explanation for this effect given by McNamara (private communication) is that proper-motion measurements of crowded stars can be significantly less precise. Thus crowded cluster members may be labeled as field stars.

A detailed analysis of the stars measured by McNamara *et al.* is enlightening. (Hereafter, star numbers reference the listing in McNamara *et al.*) If we assume that the surface-density distribution of the actual field stars is uniform, then we can estimate from the observed "field" (i.e., all stars with membership probability less than 10%) distribution the number of cluster members in the cluster core which are improperly clas-

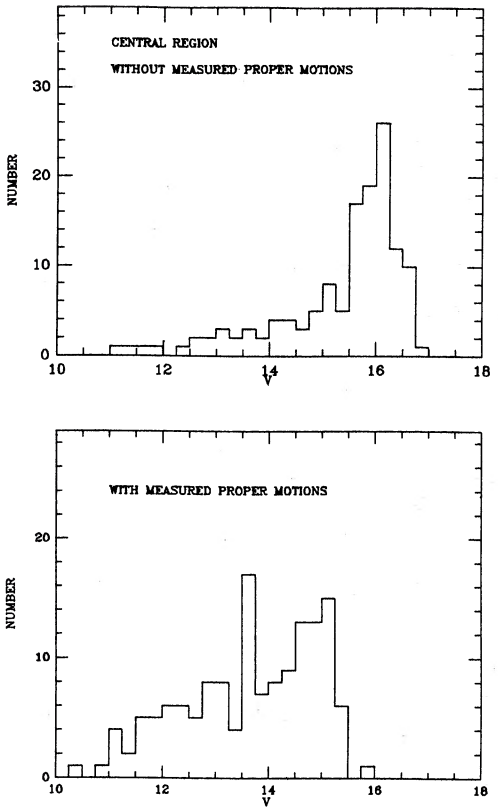

FIG. 4.—Histogram of magnitudes for stars ($V < 17$) in a selected region in the cluster core, differentiating between stars with and without measured proper motions.

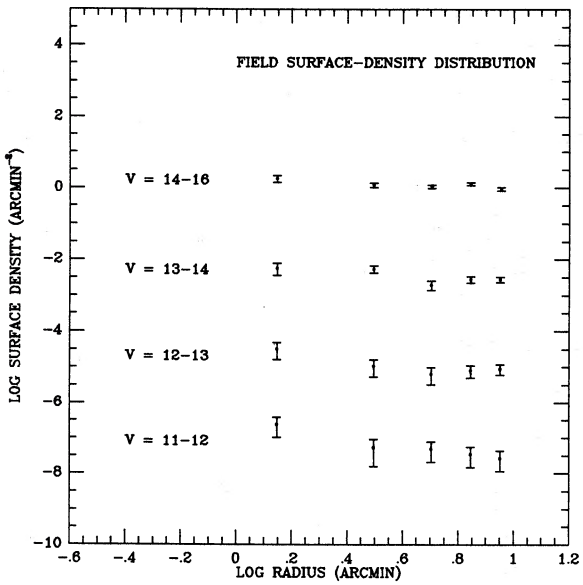

FIG. 5.—Radial surface-density distribution of field stars differentiated by luminosity. Each group has been offset in surface density from the next highest mass by two in the log. Errors are from sampling statistics.

sified as field stars. For the brightest group, $V < 12$, the observed "field" distribution suggests an excess of two to three stars in the cluster center. In fact, stars 979 (membership probability 0%) and 995 (membership probability 5%) are both badly crowded by neighbors. Object 979 is actually two stars, both brighter than $V = 12$. Similarly, there is an excess of three stars in the range $V = 12$–13. Three crowded stars are found—890, 1257, and 1292—all with membership probability 0%. For stars with $V = 13$–14, there is an excess of four stars. Three crowded stars were found—948, 1035, and 1193. Finally, there is an excess of seven stars in the range $V = 14$–15. Five crowded stars were found—754, 807, 830, 1078, and 1246. It is worth noting that many of these stars have larger measurement errors than uncrowded stars whose proper motions were determined from similar numbers of plate pairs. It thus appears likely that the central increase is in fact due to incorrect identification of cluster members as field stars. Whether in fact all of the above stars are in fact cluster members is of course unknown. However, most are located centrally in the cluster core so that the probability of membership is very high. These crowded stars are thus included in the sample of cluster members. The resultant field radial surface-density distributions are consistent with a uniform distribution.

V. LUMINOSITY FUNCTION

The differential luminosity function of M11 is given in Figure 6. The cluster has been divided into two regions, an inner region with radius $R < 2'$ (approximately 1.5 core radii; visually this is the central core) and an outer region with $R > 2'$. For each of these regions, the luminosity function is given for stars with membership probability greater than 10%, edited of field members and corrected for incompleteness. Also shown in Figure 6 are the luminosity functions of each region for stars with membership probability greater than 50%, unedited and uncorrected for completeness. The differences between the corrected and uncorrected data are not merely quantitative but qualitative as well, in that the incompleteness in the uncorrected sample masks the true rise in the luminosity function of the inner region and causes an artificial turnover in the luminosity function of the outer region.

The differential luminosity function of M11 is distinguished by two notable characteristics: (1) the slope of the inner-region luminosity function is much flatter than that of the outer region, and (2) the inner-region luminosity function does not increase indefinitely but begins to level out at the fainter magnitudes. Both of these effects were found to be present in many open clusters by van den Bergh and Sher (1960).

The relative dominance of low-mass stars over high-mass stars in the outer region of the cluster is even more marked in Figure 7, where the inner- and outer-region cumulative luminosity functions are given. Here we have included the results of the star counts, which allow study of the luminosity function to $V = 20$ but require restricting the use of proper-motion data to stars with $R < 5'$ (the effective radial limit of the star counts). Again, the inner- and outer-region cumulative luminosity functions have notably different shapes, with the more rapid rise in the number of faint stars in the outer region relative to the inner region continuing to $V = 20$.

In order to study the luminosity function of the cluster as a whole, the total cumulative luminosity function (i.e., the sum of the inner and outer regions) is also shown in Figure 7. The errors shown are from sampling statistics. Also shown is the field initial luminosity function, derived from the field initial

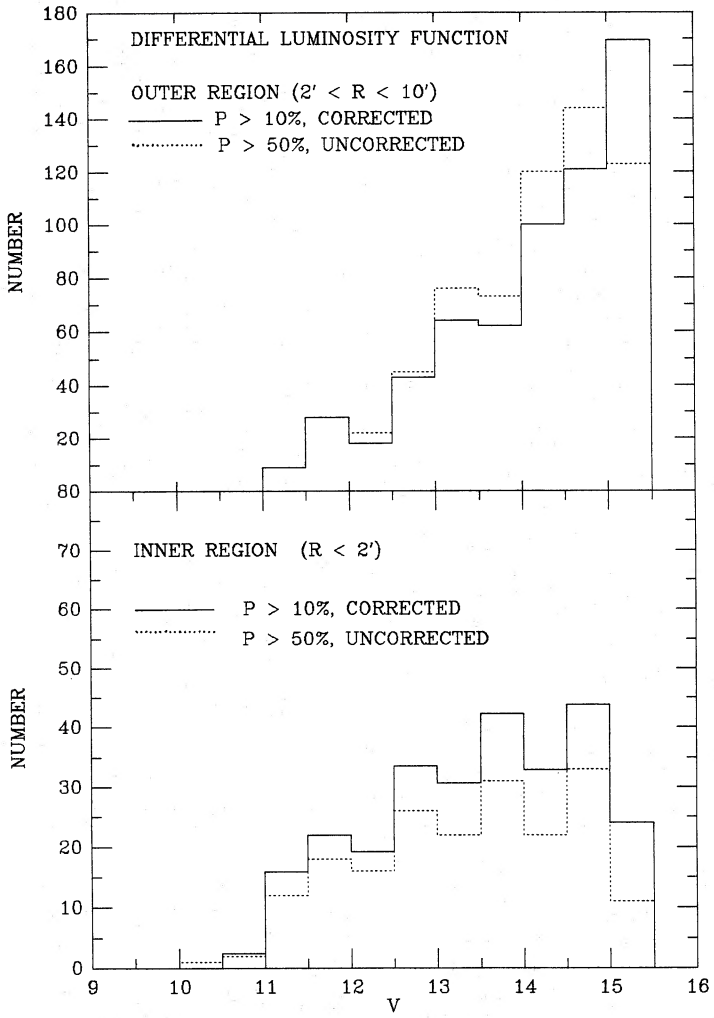

FIG. 6.—Differential luminosity function for inner and outer regions of cluster. Solid lines are the data corrected as explained in text; dashed lines are uncorrected data.

mass function given by Miller and Scalo (1979). The agreement between the two is good for stars brighter than $V = 15$ (1.6 $M_\odot$). There is, however, a deficiency in the lower mass stars relative to the field in that the total star count at $V = 20$ (0.7 $M_\odot$) is below that predicted by the field initial luminosity function. The extent of this deficiency is sensitive to several systematic effects. Incompleteness is certainly present in the star counts within the last magnitude. Also, systematic errors may be present in the limiting magnitude of the star counts and in the apparent luminosity-mass calibration.

A natural explanation of the differences in the inner- and outer-region luminosity functions, and to some extent the deficiency in the low-mass stars relative to the field, is provided by the dynamical analysis of the cluster to be done in the next section. In particular, radial surface-density profiles derived from dynamical models in energy equipartition are found to fit well the stellar distribution in the cluster. In such models, the more massive, bright stars have a higher central concentration, and the resultant model inner- and outer-region luminosity functions mimic the relative behavior of the observed luminosity functions.

These models show that a larger fraction of the lower mass stars relative to the higher mass stars is located outside the 5′ radius region. Thus studying only the stars within 5′ will underestimate the low-mass population, as observed. In fact, this effect is not sufficient to fully explain the observed deficiency in low-mass stars. We show in Figure 7 the total luminosity function of the dynamical models, normalized so as to equal the observed cumulative luminosity function at $V = 15$. The agreement with the field initial luminosity function remains good for the higher mass stars, while the deficiency in the low-mass stars is reduced by almost a half. Given also the possible systematic errors in the observed number of faint stars, the remaining deficiency in the cluster luminosity function at the faint end relative to the field must be taken with some caution.

The luminosity function derived from the proper-motion sample is comprehensive in that it extends, in terms of mass fractions, essentially to the radial limits of the cluster (90% of the mass is included, as estimated from the dynamical models of § VI). With the inclusion of the star-count data the luminosity function is also known well into the low-mass regime of the mass spectrum. It can thus be used to provide an estimate of a large fraction of the total observed mass of M11. Such an estimate was made by McNamara and Sanders (1977) using the uncorrected proper-motion data sample. The following improvements are made here. First, the membership sample is corrected as discussed above. Second, masses are obtained by fitting the main sequence to the stellar-evolution models of Patenaude (1978), adopting $E(B-V) = 0.42$ from Johnston, Sandage, and Wahlquist (1956) and using the bolometric corrections of Code *et al.* (1976). The main-sequence fitting indicates an apparent distance modulus of 12.5 and a cluster age on the order of 2×10^8 yr. Both are in reasonable agreement with previous estimates (Johnson, Sandage, and Wahlquist 1956; Solomon and McNamara 1980). Third, the star counts allow the accounting to be extended to stars with masses as low as 0.7 $M_\odot$. The total mass of stars with $15 < V < 20$ and located between 5′ and the spatial limit of the proper-motion survey was found by scaling the total number of such stars within 5′ by the density profiles of the dynamical models fitted to the cluster in the next section.

A large uncertainty in such a mass estimate is the correction for the mass of binary secondaries. Abt and Levy (1976) find that for F3–G2 IV or V field stars, binary companions have a total mass half that of the total mass of the primaries and single stars. Mathieu, Stefanik, and Latham (1985) find the binary population among such stars in the Hyades to be very similar to that in the field. Furthermore, little dependence of the binary frequency on mass has been found in either the field (Abt and Levy 1978) or the Hyades (Mathieu, Stefanik, and Latham 1985). We thus include here a factor of 1.5 correction in the total mass estimate. This is only a rough correction, however, because of uncertainties in the correction itself and because it remains unclear to what extent the binary distribution is uniform from cluster to cluster (see Abt 1983 for a review).

Table 3 shows the mass compilation, the total observed mass being 4671 $M_\odot$. The dynamical models fitted to the data in § VI suggest that 10% of the cluster mass lies outside the radial limits of our study. With this correction the mass becomes 5190 $M_\odot$. The actual mass of the cluster is certainly higher owing to the presence of stars with masses less than 0.7 $M_\odot$. If the luminosity function of M11 is similar to that in the field, as much as 40% of the cluster mass may exist in stars with masses between 0.1 $M_\odot$ and 0.7 $M_\odot$. However, the nature and uni-

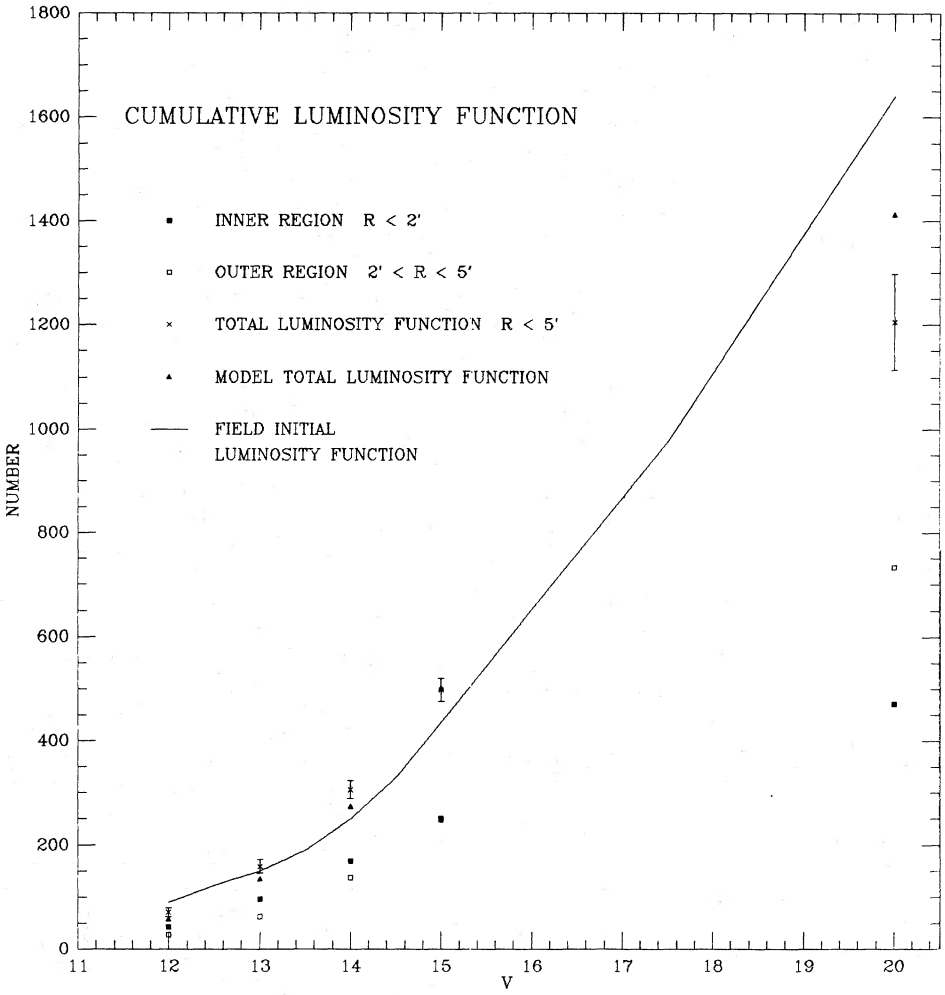

FIG. 7.—Cumulative luminosity function for inner and outer region of cluster as well as total observed luminosity function. The results of deep star counts are included at $V = 20$, limiting the radius of the outer region to 5'. Solid line is the field initial luminosity function. Model cluster total luminosity function is described in text.

formity of open cluster luminosity functions below 1 $M_\odot$ are at the moment uncertain; there is evidence that some clusters are deficient in low-mass stars relative to the field (for a review see Scalo 1984).

TABLE 3

M11 MASS DISTRIBUTION

V	N	M_*[a]	M_{TOT}
10.5–12.0			
Main sequence	45	3.5 $M_\odot$	157 $M_\odot$
Red giants	32	(4.0)[b]	128
12.0–13.0	114	2.8	319
13.0–14.0	200	2.4	480
14.0–15.5	491	1.9	933
15.5–20.0	1097	1.0	1097
			3114
Mass in binary secondaries			1557
Total observed mass.....			4671

[a] See text for source of masses.
[b] See § VI*e*.

VI. RADIAL SURFACE-DENSITY DISTRIBUTIONS AND DYNAMICS

a) Radial Surface-Density Distributions

From a dynamical point of view, the primary result to be obtained from a clean sample of cluster members is the radial surface-density distribution as a function of stellar mass. Without kinematic information, the density profiles are the only interface with the dynamics of the cluster. One inherent problem with open clusters is that the precision with which one can study the cluster structure as a function of radius and mass is limited by small-number statistics. M11 being a rich cluster, however, the problem is lessened.

The M11 radial surface-density profiles as a function of mass are given in Figure 8 and tabulated in Table 4. The data were first divided into four magnitude intervals: $V < 12.0$ ($M/M_\odot = 3.5$), 12.0–13.0 ($M/M_\odot = 2.8$), 13.0–14.0 ($M/M_\odot = 2.4$), and 14.0–15.0 ($M/M_\odot = 1.9$). The masses given are for stars of age $t = 2 \times 10^8$ yr (see § V); the 32 red giants have been included in the 3.5 $M_\odot$ group. The data were then divided into radial bins. The maximum radius of 9'.6 was defined by the spatial extent of the proper-motion study. The cluster was then divided into 20, 10, and 5 equally spaced annuli. For any given luminosity group, high-resolution bins were used in the core,

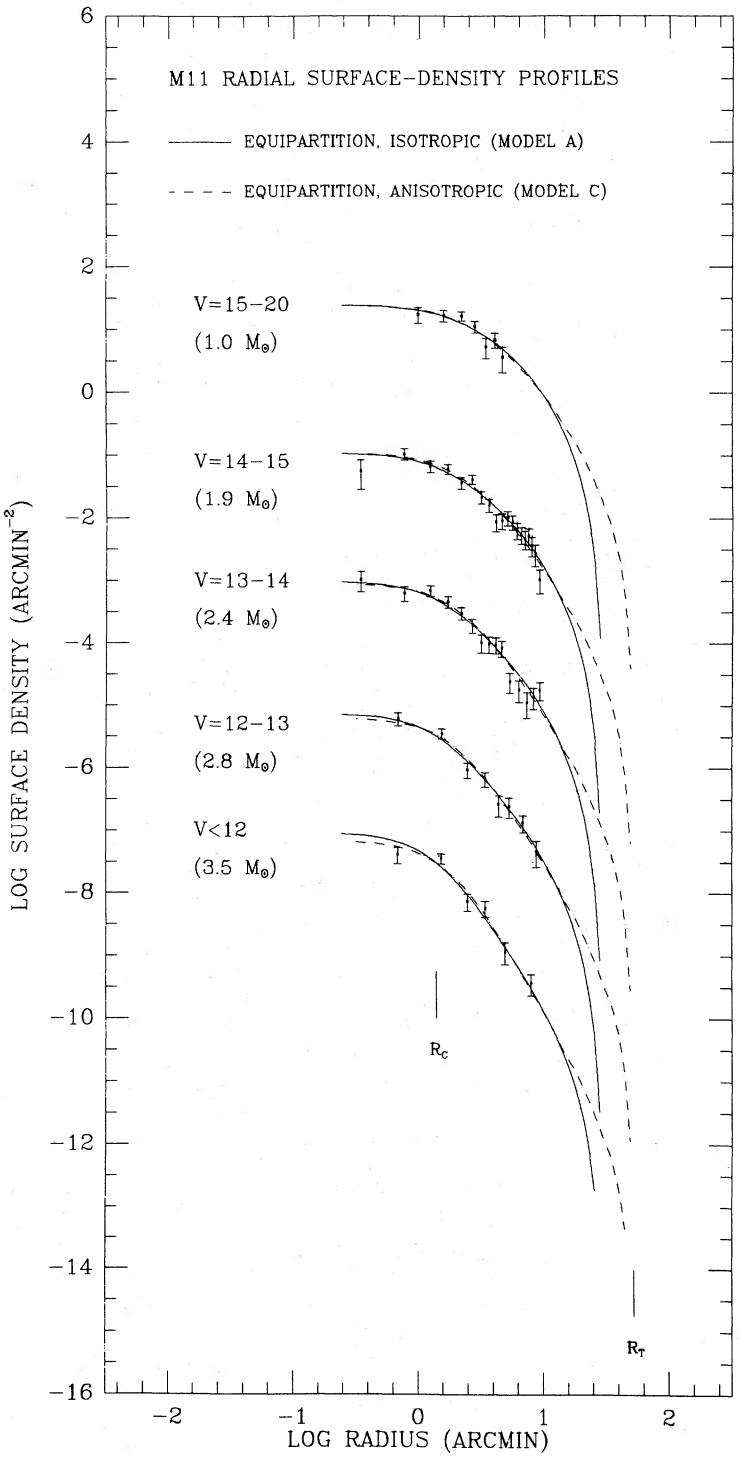

FIG. 8.—Radial surface-density distribution of cluster members, divided into five luminosity (mass) groups. Each group has been offset in surface density from the next highest mass by two in the log. Errors are due to sampling statistics. Curves are best fit isotropic and anisotropic King models. R_C is the core radius of the isotropic model; R_T is the theoretical cluster tidal radius.

TABLE 4

TABULATED RADIAL SURFACE-DENSITY PROFILES

R (')[a]	Surface Density (arcmin^{-2})	σ
$V < 12$ (3.5 $M_\odot$)		
0.69.....	4.13E+00	1.18E+00
1.53.....	3.57E+00	6.35E−01
2.47.....	7.44E−01	2.24E−01
3.43.....	5.79E−01	1.67E−01
4.95.....	1.18E−01	4.47E−02
8.00.....	3.70E−02	1.40E−02
$12 < V < 13$ (2.8 $M_\odot$)		
0.69.....	6.09E+00	1.44E+00
1.53.....	3.52E+00	6.30E−01
2.47.....	9.47E−01	2.53E−01
3.43.....	6.77E−01	1.81E−01
4.39.....	2.63E−01	9.93E−02
5.36.....	2.46E−01	8.72E−02
6.86.....	1.33E−01	4.01E−02
8.78.....	4.70E−02	2.10E−02
$13 < V < 14$ (2.4 $M_\odot$)		
0.34.....	1.04E+01	3.75E+00
0.77.....	6.35E+00	1.69E+00
1.24.....	6.93E+00	1.37E+00
1.71.....	4.70E+00	9.54E−01
2.20.....	3.08E+00	6.80E−01
2.68.....	1.97E+00	4.92E−01
3.16.....	1.04E+00	3.29E−01
3.65.....	9.91E−01	2.99E−01
4.13.....	9.55E−01	2.76E−01
4.61.....	8.54E−01	2.47E−01
5.36.....	2.46E−01	8.71E−02
6.32.....	1.82E−01	6.87E−02
7.29.....	1.13E−01	5.05E−02
8.26.....	1.39E−01	5.25E−02
9.23.....	1.78E−01	5.65E−02
$14 < V < 15$ (1.9 $M_\odot$)		
0.34.....	5.56E+00	2.74E+00
0.77.....	1.05E+01	2.17E+00
1.24.....	6.67E+00	1.34E+00
1.71.....	6.08E+00	1.08E+00
2.20.....	3.71E+00	7.45E−01
2.68.....	4.18E+00	7.16E−01
3.16.....	2.18E+00	4.76E−01
3.65.....	1.62E+00	3.82E−01
4.13.....	8.75E−01	2.63E−01
4.61.....	9.26E−01	2.56E−01
5.09.....	1.03E+00	2.57E−01
5.58.....	8.82E−01	2.27E−01
6.07.....	6.49E−01	1.88E−01
6.55.....	5.51E−01	1.65E−01
7.04.....	4.66E−01	1.48E−01
7.52.....	5.23E−01	1.50E−01
8.01.....	3.68E−01	1.23E−01
8.49.....	2.71E−01	1.02E−01
9.23.....	1.06E−01	4.38E−02
$15 < V < 20$ (1.0 $M_\odot$)		
0.98.....	1.75E+01	4.91E+00
1.60.....	1.66E+01	3.44E+00
2.20.....	1.67E+01	2.81E+00
2.82.....	1.14E+01	2.36E+00
3.44.....	5.43E+00	1.94E+00
4.06.....	6.99E+00	1.82E+00
4.68.....	3.71E+00	1.65E+00

[a] RMS radius for each annulus.

and the next lowest resolution bins were used in the halo. Excepting a few instances, every bin contained at least seven stars. The errors given in Figure 8 and Table 4 are from sampling statistics.

Also shown in Figure 8 is the radial surface-density distribution of all stars with $V = 15.0$–20.0 ($M/M_\odot \sim 1.0$). These were found by differencing the star counts and the cumulative proper-motion counts. As noted above, the star-count method cannot provide information as far radially as the proper motions. Nonetheless, these points provide a constraint on the mass and distribution of the lower mass stars.

A preliminary examination of the radial surface-density distribution shows M11 to be very similar to globular clusters. In fact, the density distribution integrated over mass (dominated by the lower mass stars) is well fitted by a single-mass King model of central concentration $c = 1.2$, typical of low central-concentration globular clusters. Of course, M11 does have a significant mass spectrum, which plays an important role in the dynamics of the cluster. This is evident in the marked increase in the central concentration of the higher mass groups, previously noted by McNamara and Sanders (1977). The cumulative distributions of the four components derived from the proper-motion study are shown in Figure 9. Here the mass segregation is particularly evident, although the 2.4 $M_\odot$ component has a somewhat unusual distribution in the outer region. A two-sample Kolmogorov-Smirnov test rejects the 3.5 $M_\odot$ group as deriving from the same distribution as the 2.8, 2.4, and 1.9 $M_\odot$ groups at the 90%, 98%, and 99% confidence levels, respectively. Similarly, the 2.8 $M_\odot$ group is different from the 1.9 $M_\odot$ group at the 99% confidence level, and the 2.4 $M_\odot$ group is different from the 1.9 $M_\odot$ group at the 85% confidence level. The 2.8 $M_\odot$ group is not distinguishable from the 2.4 $M_\odot$ group at a statistically significant level. Such differences in the central concentration with mass are expected from general energy-equipartition arguments. However, more detailed information about the cluster dynamics can be obtained by fitting theoretical models to the surface-density profiles.

b) *Preliminary Dynamical Model*

As discussed in the Introduction, the dynamics of open clusters is a difficult theoretical problem, and as yet no complete solution exists. Therefore, as a preliminary step in understanding the M11 surface-density profiles, multi-mass isotropic King models were fitted to the data. (See King 1966, Da Costa and Freeman 1976, and Gunn and Griffin 1979 for a discussion and detailed study of these models.) For each stellar species of mass m_i, these models assume a lowered Maxwellian for the distribution function of position and velocity:

$$f_i(r, v) = k \exp [2j_i^2 V(0)] [\exp (-2j_i^2 E) - 1] , \quad (1)$$

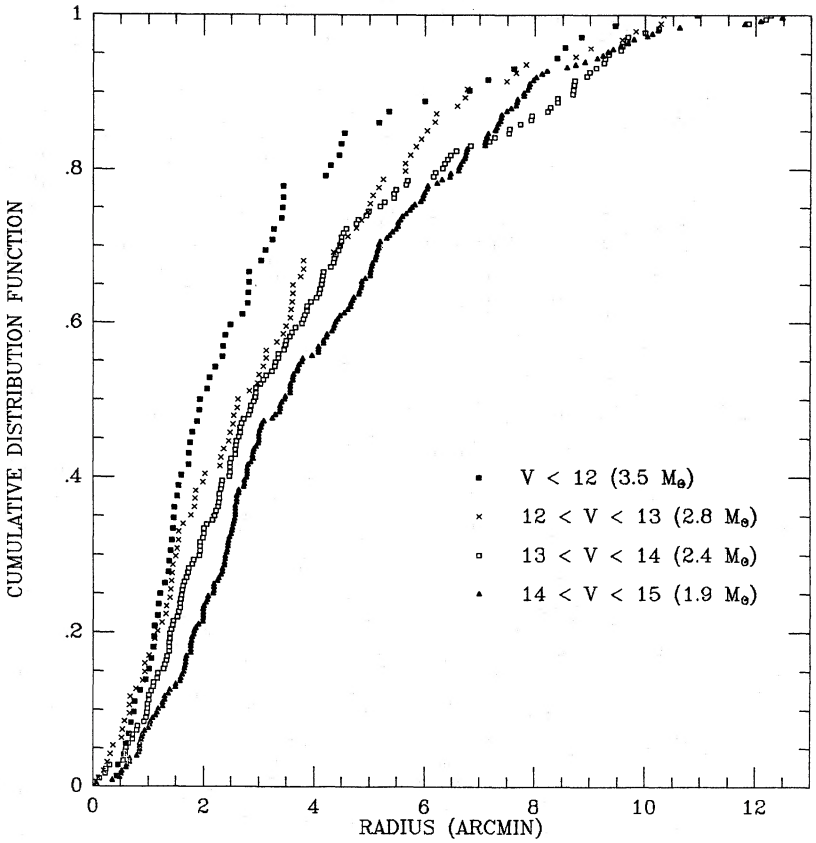

FIG. 9.—Cumulative radial distributions of the upper four luminosity groups in Fig. 8

where $V(r)$ is the potential, and $E = (\frac{1}{2})v^2 + V(r)$. The factor j_i is the modulus of precision for stellar component i. These models have finite radii, usually identified in the case of star clusters with the tidal limit imposed by the gravitational field of the Galaxy (King 1966).

When in the following analyses we assume equipartition of energy between species, it is in the sense that

$$m_i/j_i^2 = m_k/j_k^2 \ . \qquad (2)$$

Note that the models assume that the modulus of precision j is not a function of radius. Since relaxation occurs more rapidly in the central regions (Spitzer and Hart 1971*b*), this is a simplified description of the actual conditions in the cluster.

The equipartition models fitted to the data have seven free parameters: the depth of the central potential (characterized by the quantity W_0 [see Gunn and Griffin 1979; however, the value quoted here for a given model is referenced to the component comprised of the most massive stars]), the tidal radius R_T, the relative central densities of each of the five mass groups and the total central density. The stellar mass of each group is determined independently from the stellar luminosity, as given above.[3] When non-equipartition models are considered, the velocity dispersions allowed to vary become additional free parameters.

The best-fit model was found with a seven-dimensional grid search for the minimum χ^2. Tests of the model behavior show that for given values of W_0 and R_T, variations in the relative values of the central densities within a range several times larger than the errors in the data do not markedly affect the shape of the model surface-density profiles. Thus in the following analyses we discuss the variation in χ^2 only for the two-dimensional W_0-R_T space, taking for each value of W_0 and R_T the best fit values of the central densities.

c) *Mass Segregation and Energy Equipartition*

That mass segregation exists in open clusters has been recognized for some time. To what extent this reflects the presence of complete energy equipartition among the different-mass stars is not as clear. The direct measurement of differential effects in the velocity dispersions as a function of mass is extremely difficult because of the low absolute values of the dispersions in open clusters. Considering M11 in particular, McNamara and Sanders (1977) attempted to measure the velocity dispersion as a function of mass, using their very high quality (group 3)

[3] Adopting for the stellar mass of each component the median mass of single stars in the particular luminosity range is a simplification. No correction is made for (1) the presence of a range of stellar masses within each luminosity interval and (2) the presence of binaries. The latter is important because observed "single stars" of given luminosity may actually represent a range in total stellar mass; furthermore, the average mass at a given luminosity will be larger than that of a single star of that luminosity. However, we note that only the relative stellar masses of the components are important in determining the model profiles. Thus our simplification is reasonable if the proportional increase in the average mass of an observed star at a given luminosity over a single star at that luminosity is relatively independent of stellar mass. As already noted in § V, studies of both the field and the Hyades suggest that the nature of the binary population is in fact not strongly dependent on mass; thus the assumptions made here are reasonable. In the following, for simplicity, we will refer to each stellar component by the median mass of a single star in the respective luminosity range; in fact, the average mass of the stars in each luminosity range will be somewhat higher.

TABLE 5

χ^2 FOR EQUIPARTITION ISOTROPIC KING MODELS

	TIDAL RADIUS (pc)																	
W_0	8	9	10	11	12	13	14	15	16	17	18	19	20	21	22	23	24	25
7.....	112	74	78	102														
8.....		88	60	59	74	98												
9.....			87	60	49	52	63	81										
10.....				101	75	57	49	48	53	62								
11.....							78	70	61	55	53	55	59	67	77			
12.....											83	78	73	69	67	66	67	71

proper-motion data. They find little dependence of the velocity dispersion on mass and suggest that energy equipartition is not present in the cluster. Thus, as our initial dynamical model, we assume the case where the velocity dispersions of all the stars are the same. In most dynamical models, and King models in particular, the consequence of uniform velocity dispersion across mass is identical radial surface-density profiles for each mass group. This clearly is not the case in M11. For all values of W_0, such models are rejected at confidence levels of 99% or higher. The rejection is largely due to a very poor fit of the 3.5 $M_\odot$ component. However, even excluding this component, it is not possible to find a model which fits all of the lower mass components well. These components alone reject all models at the 90% confidence level or better.

Given that models with no energy equipartition do not fit the data well, we next consider the case of complete energy equipartition. Fitting isotropic equipartition King models to the data, we obtain the array of χ^2 values given in Table 5. Clearly, these models can fit the data very well. The best fit model, hereafter referred to as model A, has $W_0 = 10$ and $R_T = 15$ pc. With 48 degrees of freedom in the fit, model A has a reduced χ^2 of 1.0. The radial surface-density profiles of model A are given in Figure 8, and specifications and details of the model are given in Table 6. The core radius of the model is 0.72 pc. (Here core radius is defined by the analog of eq. [15] in King 1966 for multi-mass models; see, for example, Gunn and Griffin 1979.)

Both the tidal radius and the central potential are well constrained by the data. Models with χ^2 greater than 62 can be rejected at the 95% confidence level (Lampton, Margon, and Bowyer 1976). Thus the 95% confidence interval of the tidal-radius estimate ranges from 10 pc to 20 pc. Similarly, W_0 is constrained to values between 8 and 11. The upper constraint on W_0 is due primarily to the degree of mass segregation rather than to any curvature in the halo of the cluster (as is the case in globular clusters, for example). The 95% confidence interval on the core radius ranges from 0.57 pc to 0.88 pc.

Thus an isotropic model in complete equipartition is quite consistent with the data. An alternative possibility is that energy equipartition has not carried through entirely to completion. In Monte Carlo simulations with mass distributions somewhat more dominated by massive stars than in M11, Spitzer and Shull (1975) find that the exact mass of the lighter stars does not much affect the degree of spatial segregation of these lighter stars relative to the massive stars. In order to determine to what extent this might be the case in M11, non-equipartition models were fitted to the data. The data are entirely insufficient to constrain a model with five velocity dispersions as free parameters, so only certain interesting cases were studied. First, the velocity dispersions of the four lower mass components were forced to be identical, with the given velocity dispersion ranging from that of 1 $M_\odot$ to 2.8 $M_\odot$ stars in equipartition. These models were rejectable at the 98% confidence level or better for all values of W_0, R_T, and the low-mass velocity dispersion. The rejection is entirely due to poor fits among the lower mass components. Any one central concentration cannot fit all of them well. For any given W_0, the best fit values of R_T are compromises between the best fits for the 2.8 and 2.4 $M_\odot$ groups and the 1.9 and 1.0 $M_\odot$ groups.

TABLE 6

SPECIFICATIONS AND DETAILS OF BEST FIT KING MODELS

	MODEL		
PARAMETER	A	B	C
W_0	10	8	8
R_T	15 pc	14 pc	25 pc
R_A[a]	...	...	2.81
$M_{\mathrm{relax},i}$[b]	1.00	1.00	1.00
	0.80	0.80	0.80
	0.69	0.69	0.69
	0.54	0.69	0.54
	0.29	0.69	0.29
$\rho_{0,i}$[c]	165 $M_\odot$ pc^{-3}	105 $M_\odot$ pc^{-3}	109 $M_\odot$ pc^{-3}
	90	64	70
	92	72	79
	69	88	67
	61	133	61
$M_{\mathrm{total},i}$[d]	492 $M_\odot$	471 $M_\odot$	456 $M_\odot$
	529	508	505
	837	792	796
	1077	981	1041
	2272	1477	2204
$R_{1/2,i}$[e]	1.0 pc	1.1 pc	1.0 pc
	1.4	1.5	1.4
	1.7	1.7	1.5
	2.0	1.7	1.9
	2.6	1.7	2.7
R_{quint}[f]	1.2 pc	1.0 pc	1.3 pc
	2.1	1.8	2.1
	3.2	2.6	3.3
	4.9	4.2	5.9
	15.0	14.0	26.0

[a] Anisotropy radius, measured in units of one core radius (0.7 pc).

[b] Relaxation mass, i.e., the mass (normalized to the largest stellar mass) of stars which in equipartition would have the velocity distribution of component i. The subscript i here and in the remaining table refers to the stellar components as described in the text, going from most to least massive (i.e., 3.5 $M_\odot$, 2.8 $M_\odot$, 2.4 $M_\odot$, 1.9 $M_\odot$, and 1.0 $M_\odot$).

[c] Central volume density; 50% correction for mass in binary secondaries has been included for each component.

[d] Total mass; 50% correction for binary mass has been included.

[e] Projected half-mass radius for each component.

[f] Radii dividing total mass into quintiles.

TABLE 7

χ^2 FOR NON-EQUIPARTITION ISOTROPIC KING MODELS

	Tidal Radius (pc)																	
W_0	9	10	11	12	13	14	15	16	17	18	19	20	21	22	23	24	25	26
6.....	87	85	103															
7.....		80	69	72	84													
8.....			96	75	65	61	65	72	84									
9.....						93	81	73	68	65	65	67	71	76	82			
10.....														85	82	80	78	78

Next, models with the velocity dispersions of only the lower three mass components held identical were fitted, taking velocity dispersions of 1.0, 1.7, and 2.4 $M_\odot$ stars in equipartition. The quality of the fits improved, the best fit model being rejectable at only the 90% confidence level. The best fit model (model B in Table 6) had $W_0 = 8$, $R_T = 14$ pc, and the three lower components at the velocity dispersion of the 2.4 $M_\odot$ component in equipartition. The distribution of χ^2 for models with the lower components having this velocity dispersion is given in Table 7. The 95% confidence level includes values of W_0 from 7 to 10 and tidal radii from 11 to 21 pc. If the lower mass components are held at the velocity dispersion of 1.7 $M_\odot$ stars in equipartition, equally good fits are obtained. Acceptable models lie within a range of W_0 between 8 and 11 and tidal radii from 10 to 18 pc. When the velocity dispersion of the lower component was set to that of 1.0 $M_\odot$ stars in equipartition, no acceptable fits were obtained.

The dependence of these conclusions on the presence of unseen mass in the cluster was checked. Complete equipartition models were fitted with a sixth component of stellar mass 0.4 $M_\odot$ and total mass of 40% that of the cluster (roughly that expected if the mass function is similar to the field initial mass function). The effect on the model fits was small, the best fit models having slightly larger tidal radii. Similarly, models were fitted with a sixth component of stellar mass 1.5 $M_\odot$ and total mass of 15% that of the cluster (simulating a population of neutron star remnants derived from the initial mass function above 4 $M_\odot$). The effect of this component on the resulting best fit parameters was insignificant.

In conclusion, then, the evidence strongly suggests that the massive stars have transferred energy to the lighter stars via two-body encounters. The data are fitted very well by models where all stars are in complete energy equipartition. However, models in which the lower mass stars all have the same velocity dispersion can only be rejected at the 90% confidence level. Nonetheless, the excellent fit of the complete energy equipartition model argues for this being nearer the actual state of the cluster members with masses greater than approximately 1 $M_\odot$.

An approximate relaxation time for the inner half of the cluster can be obtained using equation (5) of Spitzer and Hart (1971*a*). If we adopt a cluster mass of 5200 $M_\odot$, a half-mass radius of 2.5 pc (model A), and the number of cluster stars as 2000, we find a relaxation time of 4×10^7 yr. This is only a lower limit because of the presence of unseen mass in the cluster. As an upper limit we assume that the mass function is similar to the field initial mass function and adopt a cluster mass of 9000 $M_\odot$, a half-mass radius of 2.9 pc (from model fits with a sixth component of 0.4 $M_\odot$), and a cluster population of 10,000 stars. This gives a relaxation time of 1.3×10^8 yr. These numbers provide a reasonable range of estimates on the cluster relaxation time scale. However, they are only global estimates; local relaxation times vary greatly with radius in the cluster. Furthermore, stars with masses greater than the average stellar mass in the cluster have equipartition times shorter than these relaxation times.

Even with this approximate treatment, it is clear that the relaxation time scale of M11 is less than the cluster age. Thus the presence of mass segregation in the cluster is not surprising. We also note that if we adopt a cluster velocity dispersion of roughly 2.5 km s^{-1} (McNamara and Sanders 1977; Mathieu 1983; Mathieu and Latham 1984), the crossing time of the system (i.e., the time to cross the half-mass radius) is on the order of 1×10^6 yr. Thus the average relaxation time in M11 is on the order of 50–100 times longer than the average crossing time.

Finally, we return briefly to the question of the dependence of velocity dispersion on stellar mass. This issue is discussed elsewhere in more detail (Mathieu 1983). Here we only note that in the presence of a tidal field, the dependence of velocity dispersion on mass is markedly reduced. Put very simply, this is because the tidal field truncates the velocity distribution of the low-mass stars more severely than the velocity distribution of the high-mass stars. In model A, for example, the global velocity dispersion of the 3.5 $M_\odot$ component is only 7% less than that of the 1.0 $M_\odot$ component. Thus the lack of any dependence of the global velocity dispersion on stellar mass observed by McNamara and Sanders (1977) may not be inconsistent with the presence of energy equipartition in M11.

d) Tidal Radius and Anisotropy

King models have a finite limiting radius, usually identified with the tidal limit imposed on a cluster by the galactic field. In the case of the best fit equipartition model, model A, this limiting radius is 15 pc. If we assume that the dominant tidal force is due to the Galaxy, then a theoretical tidal limit can be computed by adopting the formula of King (1962; see also Bok 1934) to obtain

$$R_T = (GM_{\rm clust}/4\omega A)^{1/3} .$$

Adopting for the cluster mass 5200 $M_\odot$ (in fact, a lower limit), for the angular velocity of galactic rotation, ω, 30 km s^{-1} kpc^{-1}, and for the Oort constant, A, 12 km s^{-1} kpc^{-1} (both of these for the galactic radius of M11, obtained from a smoothed galactic rotation curve [M. Fich, private communication; see also Burton 1976]), one finds $R_T = 25$ pc for M11. The difference between this theoretical value and the model values is statistically significant. The largest tidal radii within the 95% confidence level are 20 pc and 21 pc, for the equipartition and non-equipartition models, respectively. Also, the theoretical tidal radius is insensitive to the input values, and, in any case,

TABLE 8

χ^2 VALUES FOR BEST FIT ANISOTROPIC KING MODELS ($R_T = 25$ pc)

W_0	R_A[a]	χ^2
2.....	0.34	62
4.....	0.79	55
6.....	1.49	50
8.....	2.81	47
10.....	6.15	47
12.....	25	64

[a] R_A is measured in units of one core radius (0.7 pc).

the largest error in the theoretical value is probably the low mass estimate for the cluster.

The discrepancy can be resolved by removing the restriction to isotropic velocity dispersion models. As pointed out by Michie (1963), the effect of adding anistropy to a given isotropic model is to increase the central concentration. As it is the core radius which is constrained by the M11 data, this is equivalent to an increased model tidal radius.

In order to include the effect of anisotropy in the models, the lowered Maxwellian (eq. [1]) is multiplied by the factor exp $(-\beta J^2/R_A^2)$, where J is the specific angular momentum, and R_A is a characteristic radius beyond which the effects of anisotropy become important (Michie 1963). (Note that R_A is assumed independent of mass.) For models with values of R_A on the order of a core radius or greater, the differences in the model density distributions from the isotropic case are small out to the radial limits of the M11 data. Thus, the data are unable to actually determine the value of R_A. However, forcing the models to have tidal radii equal to the theoretical tidal limit is a severe constraint on R_A for any given W_0. Table 8 gives the values of χ^2 in W_0-R_A space for a fixed tidal radius of 25 pc. (In Table 8 and the following, R_A is given in units of core radii, roughly 0.7 pc.) As χ^2 is very sensitive to the choice of R_A (for given W_0 and R_T), only the best fit values are presented. As expected, the best fit anisotropic models, with R_A on the order of several core radii, fit as well as the isotropic models, since in the region of the data the two are essentially identical. In Figure 8, the $W_0 = 8$ and $R_A = 2.81$ model (model C; specifications are given in Table 6) is shown as an example.

The constraint on the value of R_A is not particularly good. Because a smaller anisotropy radius somewhat compensates for a more severe tidal cutoff (W_0 smaller), excellent fit models can be obtained for lower values of W_0 than in the isotropic case. It is not until the best fit anisotropy radius moves within a core radius, well within the radial extent of the data, that the data can begin to reject models. Thus the most that can be ascertained from the radial-density profiles is that anisotropy does not seem to be significant much inside of a core radius. Whether anisotropy actually extends that far inward in the cluster is not clear.

That anisotropy would be present in the cluster is not unexpected theoretically. N-body and Monte Carlo simulations for isolated clusters have shown that the ejection of stars from cluster cores due to two-body and binary encounters creates a cluster halo of stars on predominantly radial orbits. For non-isolated clusters, this anisotropy can be reduced by tidal effects from both passing ISM clouds and the galactic field, as tidal encounters do not conserve angular momentum within the cluster (Prata 1971). The magnitude of these effects is not clear, however. On the observational side, McNamara and Sanders (1977) find in M11 that the radial velocity dispersion exceeds the tangential dispersion by a factor of 1.8 for stars between 1.5 and 3 pc (beyond which the high-precision data are exhausted). They point out, however, that the confidence level of this observation is low. With higher precision, both Jones (1970) and van Leeuwen (1980) find significant anisotropy in the Pleiades to within 1 pc of the center; similar results were found by Jones (1971) in Praesepe.

In conclusion, the presence of anisotropy is consistent with the data and necessary if the King model radial limit is to be identified with the theoretical tidal radius. It is important to realize, though, that these conclusions regarding anisotropy in M11 are strongly model dependent. There is little suggestion of a precise finite radial limit in the data; any limit is defined by the fitted King models. As will be discussed in § VI*f*, there is some uncertainty theoretically concerning the velocity distribution of the high-energy stars; it is this distribution which determines the structure and radial limit of the halo. Nonetheless, King models do fit very well the radial surface-density profiles of globular clusters, where the halo surface-density distributions are well defined. On the other side, the theoretical tidal radius considers only the galactic tidal field as determined from a smoothed rotation curve, whereas local effects (e.g., local giant molecular clouds) may play equally important roles in altering the halo structure of the cluster. Thus the presence of anisotropy is only one of several possible explanations for the difference between the theoretical tidal radius and the model-determined radial limit.

As a final point, we note that it has been found in both analytic and numerical studies that the galactic tidal field can produce significant flattening in a cluster halo along the direction normal to the galactic plane. The presence of massive interstellar clouds, however, may act to reduce this effect by not allowing the cluster to completely fill the permitted volume within the tidal radius. We have examined the M11 proper-motion data for axial symmetry by dividing the data into quadrants, the boundaries first aligned north/south and then rotated 45°. In both orientations no statistically significant deviations from axial symmetry were found. Opposing quadrants were also combined, thus comparing the radial distributions along normal axes with improved statistics; again no significant variations were found. The relevance of these negative results may not be great, however, as the data do not extend very far into the cluster halo where the tidal flattening should be most evident.

e) The Radial Distribution of Red Giants

Solomon and McNamara (1980) noted an excess of red giants relative to massive main-sequence stars in the outer regions of M11. In Figure 10, we show the cumulative radial distributions of the upper main-sequence stars ($V < 11.5$; 4 $M_\odot$) and the red giants. The two are notably different. However, a two-sample Kolmogorov-Smirnov test shows that the two stellar groups can be rejected as deriving from the same distribution at only the 90% confidence level. Thus the statistical significance of the difference in the distributions is only marginal. Both the giant and the main-sequence turnoff distributions deviate from the theoretical distribution for 4 $M_\odot$ stars; however, neither observed distribution can be rejected as

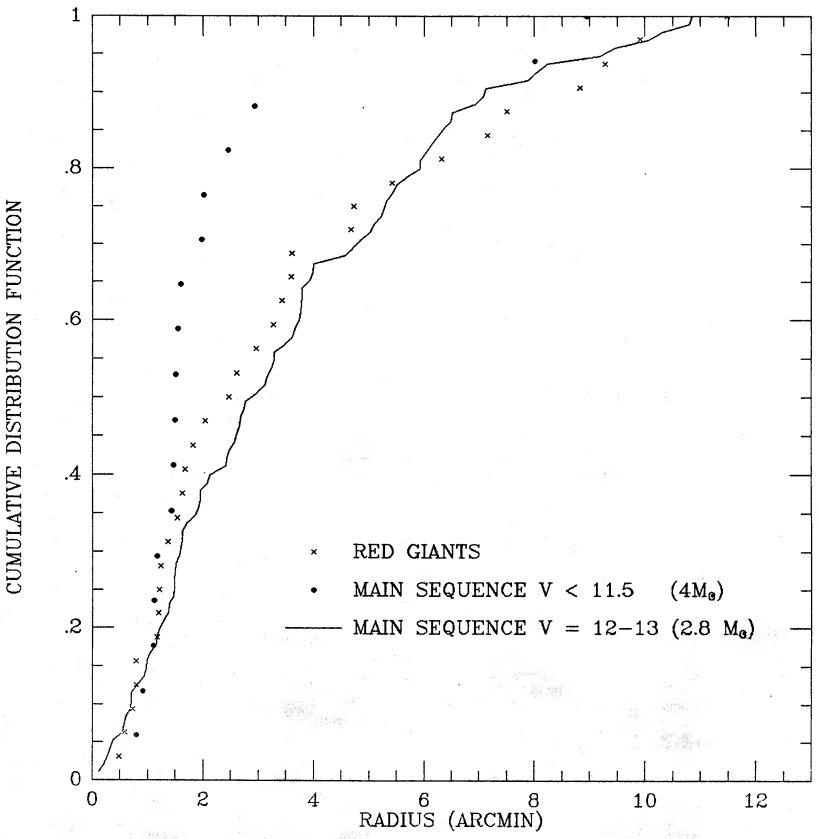

FIG. 10.—Cumulative radial distributions of the most massive (4 $M_\odot$) main-sequence stars and red giants. Solid line is the integrated radial distribution of 2.8 $M_\odot$ main-sequence stars.

deriving from the theoretical distribution at better than the 85% confidence level. (The theoretical distribution is derived by adding a trace mass of 4 $M_\odot$ stars to model A.) Nonetheless, the red-giant distribution is quite similar to the distribution of the 2.8 $M_\odot$ stars, also shown in Figure 10.

A careful check has been made to determine whether the differing distributions are a result of the membership selection procedure. Considering first stars determined to be cluster members, radial velocities have been obtained for 30 of the 32 giants (Mathieu 1983; Mathieu and Latham 1985). All but two are certain members. The remaining two are spectroscopic binaries with unknown γ velocities; as they are both located in the cluster core, they are probable cluster members. As for the proper-motion nonmembers, each field star with $V < 12.5$ was examined for possible proper-motion errors due to crowding. Several were badly crowded, but only one such star, star 979, was either a giant or an upper main-sequence star. (This star also had abnormally large measurement errors; see discussion in § IV.) Star 979 is in fact two stars, an upper main-sequence star and a red giant. Given the location of these stars in the cluster core, they are both probable members and were included in Figure 10. The remaining field stars are isolated and have large proper motions with very high precision. Finally, several stars with $V < 12$ were missed in the proper-motion study (see § IV and Fig. 4). None of these were giants, but two have $V < 11.5$. Photometry from Johnson, Sandage, and Wahlquist (1956) show one of these to be on the upper main sequence; the second is also blue, but no precise color is available. As both stars are again in the core, they have been included among the upper main-sequence stars in Figure 10.

A marked difference in the radial distribution of the red giants and of the massive main-sequence stars would be somewhat surprising, since presumably the giants have just recently evolved from stars at the upper mass end of the main sequence. If their mass remains unchanged during their evolution, they should maintain the same radial distribution regardless of their evolutionary state. An immediate conjecture would be that the giants may have lost mass during their evolution. The mass of the progenitors being 4 $M_\odot$, the red-giant lifetime is on the order of several times 10^7 yr (Iben 1967). This is comparable to the two-body relaxation timescale, so it is conceivable that if the mass were lost quickly, the radial spatial spread would increase accordingly. The rate of mass loss would have to be on the order of 10^{-8} to 10^{-7} $M_\odot$ yr^{-1} in order to remove sufficiently quickly the 0.5–1.0 $M_\odot$ indicated by the radial distribution of the giants. The present picture regarding the mass loss rates of giants like those in M11 (G5–K5, $M_V < -0.5$) is very uncertain. Riemers (1975) quotes rates on the order of 10^{-10} $M_\odot$ yr^{-1}. Drake and Linsky (1983) find from VLA continuum observations a mass loss rate for β Gem (K0 III) and Arcturus (K2 IIIp, Population II) on the order of 1×10^{-10} $M_\odot$ yr^{-1}. They also find similar upper limits on the mass loss rates for several other G and K giants. Finally, giants of this type generally show no circumstellar features or line asymmetries in Ca II, features which are usually associated with high mass loss rates (Riemers 1977; Stencel 1978; but see Baliunas, Hartmann, and Dupree 1983, who detect Ca II asymmetries in the four Hyades K0 giants). However, asymmetries do appear in Mg II for the cooler giants (Mullan and Stencel 1982), which indicates the mass loss is present at lower rates. The indication then is that

the mass loss rates are not generally sufficient to explain any radial extension of the giants. It remains possible that the mass loss rates of these giants vary during their evolution and were markedly higher at an earlier stage. The detailed picture regarding giant mass loss is simply too uncertain at present to draw definitive conclusions.

Solomon and McNamara (1980) suggested that the extended giant distribution indicated that the star formation in M11 was neither co-spatial nor coeval. They suggest that moderate-to-low–mass stars formed initially in the outer regions. On the order of 10^7 yr later, further star formation occurred, producing the presently observed giant stars in the core. This picture has dynamical difficulties in that the cluster has existed for on the order of two to six relaxation times; thus it would be expected that dynamical evolution would strongly modify the formation state of the cluster. This is particularly true for the massive stars, which relax more rapidly. On the other hand, relaxation times increase markedly with radius, so that the rate of approach to equilibrium can vary with stellar energy. The general question of how long the formation characteristics of a cluster will survive is as yet unanswered and worthy of attention.

The statistical significance of the distinction between the giants and the turnoff stars being marginal, however, the distribution may simply be a statistical anomaly. Tinsley and King (1976) note a similar situation in M67, where the giants at the upper end of the giant branch have a more extended radial distribution than the giants lower on the branch. However, in this case the giant distribution is also markedly more extended than the low-mass main-sequence stars and does not appear to be relaxed. That the situations are related is thus not clear. Unable to find a satisfactory explanation, Tinsley and King concluded that despite significant confidence levels, the extended red-giant distribution in M67 is purely statistical. However, McClure and Twarog (1977) find a similar situation in NGC 188. Finally, Harwarden (1975) compared the red giant and main-sequence distributions in five old open clusters. He found that the most luminous red giants always had more extended distributions, although in only one cluster was the distinction statistically significant. In all of these cases, however, the clusters are very old, as compared to the intermediate age of M11.

f) *General Comments on Dynamics of Open Star Clusters*

As always, statistical methods test only the consistency of a model with the data, not the validity of the model as a description of the true situation. That King models fit the stellar distribution of M11 does not necessarily imply that the velocity distribution of the cluster is in fact a lowered Maxwellian. The lowered Maxwellian is an excellent approximate solution to the Fokker-Planck equation in the square-well potential approximation. However, for isolated systems Davoust (1978) and Cohn (1979) find that the velocity distribution satisfying the Fokker-Planck equation decreases to zero more rapidly at smaller energies than the linear decrease of a lowered Maxwellian. Davoust, searching for analytic fitting functions for assorted numerical simulations, suggests a quadratic energy cutoff in the velocity distribution, while Cohn finds an energy cutoff lying between a linear and quadratic cutoff to be the best fit to numerical solutions of the Fokker-Planck equation. This decrease in the tail of the velocity distribution below a Maxwell-Boltzmann is due to incomplete relaxation. To what extent these high-energy stars survive in the presence of a tidal field is unclear. It is quite possible that in low central-concentration systems such as open clusters, where the tidal field strongly truncates the velocity distribution, the lowered Maxwellian becomes a good model for the velocity distribution.

Optimally, one would of course like to determine the nature of the velocity distribution in open clusters directly from observation. However, because of the low numbers of stars in the halo (and the limited extent of most proper-motion studies), this is a difficult task. The M11 data, for instance, are unable to distinguish between reasonable velocity distributions; models built from velocity distributions with quadratic energy cutoffs fit the data as well as the King models discussed above. Thus at present the strongest argument for the use of the lowered Maxwellian in open clusters is by analogy to globular clusters, where King models fit the observed surface-density distributions better than models derived from velocity distributions with quadratic energy cutoffs.

Two more fundamental difficulties in the application of King models to open clusters may exist. First, the Fokker-Planck equation itself is not valid for systems of few members because it does not consider finite velocity changes due to close encounters, which become significant for low-N systems. Second, in order to find the density distribution consistent with a given lowered Maxwellian velocity distribution, King (1966) assumes that in solving the Liouville-Boltzmann equation, the Boltzmann term $(df/dt)_{\text{encounter}}$ can be set equal to 0, leaving only the Liouville equation to be solved. This assumption is valid for large-N systems, where the relaxation time is much longer than the crossing time, and thus energy and angular momentum are conserved along an orbit. However, for systems of small number the relaxation time and crossing times are similar; for these systems the full Liouville-Boltzmann equation must be solved self-consistently.

The first difficulty, that of discrete energy changes in two-body encounters, has been handled via the Kolmogorov-Feller equation by Retterer (1979). Solving this equation numerically, Retterer finds that the velocity distribution does not differ greatly from the lowered Maxwellian, except near the escape velocity, where the distribution is somewhat more populated than in the lowered Maxwellian distribution. As for the second difficulty, arguments can be made that deviations from solutions of the Liouville equation alone (e.g., King models) will not appear until the number of stars is very small. (See, for example, Spitzer and Hart 1971*a*, who find that for a system of as few as 100 stars the average relaxation time still exceeds the average crossing time by a factor 2.5.) That M11, a system of several thousand stars, is well fitted by King models may also be evidence to this effect. However, the magnitude of the deviation between the density distributions of low-N and high-N systems may be too small to actually distinguish the proper solution from King models with the inherently sparse data in galactic clusters.

In conclusion, the fact that multi-mass King models provide excellent fits to the M11 data is operationally of value for future research and an indication that in a general sense rich open clusters are not dynamically very different from systems with much larger numbers of stars. Furthermore, our results indicate that the variation in central concentration with stellar mass observed in open clusters is fully consistent with a dynamical system in or approaching energy equipartition, as would be expected of a system which has existed several relaxation times. This result is unlikely to be strongly model-

dependent. The details of the dynamics in open clusters, however, remain an open question, particularly with regard to the effect of differing relaxation times with radial distance in the cluster and the effect of commensurate crossing and relaxation times on the cluster velocity distribution and structure. These questions await both a better theoretical understanding and improved studies of the structure of open cluster halos.

VII. CONCLUSIONS

The conclusions to be drawn from this work fall into two categories: general procedures for determining open-cluster membership, and the structure and dynamics of one particular open cluster M11. With regard to procedures, the key point is that while comprehensive proper-motion studies are essential for the determination of cluster membership, they are not sufficient to obtain a relatively complete and pure sample of cluster members—particularly when the measurements are of average precision and/or the cluster is superposed on a rich field. In this paper, we have used location in the color-magnitude diagram as a second independent membership criterion. A significant number of field stars were found in "cluster" samples defined solely by a proper-motion membership lower limit. This contamination increases with distance from the cluster center, fainter magnitude, and poorer proper-motion precision. For proper-motion data that are not of uniformly high quality, only stars of very low membership probability (e.g., less than 10%) should be excluded on the basis of proper-motion information alone. The remaining stars are then edited of field members through the use of color-magnitude information to produce a relatively complete and pure sample of cluster members.

On the dynamical side, the essential result is that the radial surface-density profiles of M11 are well fitted by multi-mass King models with energy equipartition and anisotropy in the outer regions (the latter necessary only if we demand that the King model tidal radius agree with the theoretical tidal radius). The cluster structure is thus consistent with the dynamical theory developed for systems of large number. Complete energy equipartition models best fit the data. Models in which equipartition is not yet complete among the lowest mass stars are only rejectable at the 90% confidence level. The data reject models in which anisotropy in the velocity distribution extends much within a core radius of the cluster center; however, the surface-density profiles cannot precisely determine the degree of anisotropy in the cluster.

Finally, the red giants of M11 have an extended radial distribution relative to the main-sequence turnoff stars. The giant distribution is more in accord with that of 2.8 $M_\odot$ stars rather than the distribution of the main-sequence turnoff (4 $M_\odot$) stars. The statistical significance of the distinction between the main-sequence turnoff stars and the red giants is marginal, however. If the distinction is real, it is not easily explained by either red-giant mass loss or spatial variations in the formation times of the cluster stars.

The author would like to sincerely thank Dr. Ivan King for his counsel and support throughout this work. Dr. B. McNamara has been immensely helpful, both in providing data in machine-readable form and in providing insight into the mysteries of proper-motion measurement. Drs. H. Spinrad and J. Stauffer provided the 4 m plates. Helpful conversations with Drs. G. Basri, S. Drake, A. Dupree, L. Hartmann, L. Kuhi, J. Retterer, E. Scott, J. Silk, H. Spinrad, and J. Stauffer are gratefully acknowledged. This work has been supported by NSF grant AST 80-20606.

REFERENCES

Abt, H. 1983, *Ann. Rev. Astr. Ap.*, **21**, 343.
Abt, H., and Levy, S. 1976, *Ap. J. Suppl.*, **30**, 273.
———. 1978, *Ap. J. Suppl.*, **36**, 241.
Baliunas, S., Hartmann, L., and Dupree, A. K. 1983, *Ap. J.*, **271**, 672.
Bok, B. 1934, *Harvard Circ.*, No. 384.
Burton, W. B. 1976, *Ann. Rev. Astr. Ap.*, **14**, 275.
Chiu, G., and van Altena, W. 1981, *Ap. J.*, **243**, 827.
Code, A. D., Davis, J., Bless, R. C., and Brown, R. H. 1976, *Ap. J.*, **203**, 417.
Cohn, H. 1979, *Ap. J.*, **234**, 1036.
Da Costa, G. S., and Freeman, K. C. 1976, *Ap. J.*, **206**, 128.
Davoust, E. 1977, *Astr. Ap.*, **61**, 391.
Drake, S. A., and Linsky, J. L. 1983, *Ap. J. (Letters)*, **274**, L77.
Gunn, J. E., and Griffin, R. F. 1979, *A.J.*, **84**, 752.
Harwarden, T. G. 1975, *M.N.R.A.S.*, **173**, 223.
Iben, I. 1967, *Ann. Rev. Astr. Ap.*, **5**, 571.
Johnson, H. L., Sandage, A. R., and Wahlquist, H. O. 1956, *Ap. J.*, **124**, 81.
Jones, B. F. 1970, *A.J.*, **75**, 563.
———. 1971, *A.J.*, **76**, 470.
King, I. R. 1962, *A.J.*, **67**, 471.
———. 1966, *A.J.*, **71**, 64.
King, I. R., Hedemann, E., Jr., Hodge, S. M., and White, R. E. 1968, *A.J.*, **73**, 456.
Lampton, M., Margon, B., and Bowyer, S. 1976, *Ap. J.*, **208**, 177.
Mathieu, R. D. 1983, Ph.D. thesis, University of California, Berkeley.
Mathieu, R. D., and Latham, D. W. 1985, in preparation.
Mathieu, R. D., and Spinrad, H. 1981, *Ap. J.*, **251**, 485.
Mathieu, R. D., Stefanik, R., and Latham, D. W. 1985, in preparation.
McClure, R. D., and Twarog, B. A. 1977, *Ap. J.*, **214**, 111.
McNamara, B. J., Pratt, N. M., and Sanders, W. L. 1977, *Astr. Ap. Suppl.*, **27**, 117.
McNamara, B. J., and Sanders, W. L. 1977, *Astr. Ap.*, **54**, 569.
McNamara, B. J., and Schneeberger, T. J. 1978, *Astr. Ap.*, **62**, 449.
Michie, R. W. 1963, *M.N.R.A.S.*, **126**, 499.
Miller, G., and Scalo, J. M. 1979, *Ap. J. Suppl.*, **41**, 513.
Mullan, D. J., and Stencel, R. E. 1982, in *Advances in Ultraviolet Astronomy: Four Years of IUE Research*, ed. Y. Kondo, J. M. Mead, and R. D. Chapman (NASA Conf. Pub. 2238), p. 235.
Patenaude, N. 1978, *Astr. Ap.*, **66**, 225.
Prata, S. 1971, *A.J.*, **76**, 1017.
Retterer, J. M. 1979, *A.J.*, **84**, 370.
Riemers, D. 1975, in *Problems in Stellar Atmospheres and Envelopes*, ed. B. Baschek, W. H. Kegel, and G. Traving (Berlin: Springer), p. 229.
———. 1977, *Astr. Ap.*, **57**, 395.
Sanders, W. L. 1971, *Astr. Ap.*, **14**, 226.
Scalo, J. 1984, *Fundamentals of Cosmic Physics*, in preparation.
Solomon, S. J., and McNamara, B. J. 1980, *A.J.*, **85**, 432.
Spitzer, L., and Hart, M. H. 1971*a*, *Ap. J.*, **164**, 399.
———. 1971*b*, *Ap. J.*, **164**, 483.
Spitzer, L., and Shull, J. M. 1975, *Ap. J.*, **82**, 978.
Stencel, R. E. 1978, *Ap. J. (Letters)*, **223**, L37.
Tinsley, B. M., and King, I. R. 1976, *A.J.*, **81**, 835.
Upgren, A. R., and Weis, E. W. 1977, *A.J.*, **82**, 978.
Upgren, A. R., Weis, E. W., and DeLuca, E. E. 1979, *A.J.*, **84**, 1586.
van den Bergh, S., and Sher, D. 1960, *Pub. David Dunlap Obs.*, **2**, 203.
van Leeuwen, F. 1980, in *IAU Symposium 85, Star Clusters*, ed. J. Hesser (Dordrecht: Reidel), p. 157.

Note added in proof.—It is worth pointing out that even with the addition of photometric information, the membership determination of group 1 stars is still rather uncertain. Thus in the dynamical analyses, only stars from the proper-motion study with $V < 15$ were included, effectively excluding most group 1 stars from the sample.

ROBERT D. MATHIEU: Center for Astrophysics, 60 Garden St., Cambridge, MA 02138